U.S. DEPARTMENT OF COMMERCE
National Technical Information Service

PB-253 437

LABORATORY SIMULATION OF PLUME DISPERSION FROM LEAD SMELTER IN GLOVER, MISSOURI, IN NEUTRAL AND STABLE ATMOSPHERE

FLOW RESEARCH, INCORPORATED

PREPARED FOR
ENVIRONMENTAL PROTECTION AGENCY

APRIL 1975

160140

PB 253 437

EPA-450/3-75-066

April 1975

LABORATORY SIMULATION OF PLUME DISPERSION FROM LEAD SMELTER IN GLOVER, MISSOURI, IN NEUTRAL AND STABLE ATMOSPHERE

REPRODUCED BY
NATIONAL TECHNICAL
INFORMATION SERVICE
U. S. DEPARTMENT OF COMMERCE
SPRINGFIELD, VA. 22161

U.S. ENVIRONMENTAL PROTECTION AGENCY
Office of Air and Waste Management
Office of Air Quality Planning and Standards
Research Triangle Park, North Carolina 27711

EPA-450/3-75-066

LABORATORY SIMULATION OF PLUME DISPERSION FROM LEAD SMELTER IN GLOVER, MISSOURI, IN NEUTRAL AND STABLE ATMOSPHERE

by

Hsien-Ta Liu and Jung-Tai Lin

Flow Research, Incorporated
1819 S. Central Avenue
Kent, Washington 98031

Contract No. 68-02-1294
Program Element No. 2AC129

EPA Project Officers: Edward Burt and Charles Whitmore

Prepared for

ENVIRONMENTAL PROTECTION AGENCY
Office of Air and Waste Management
Office of Air Quality Planning and Standards
Research Triangle Park, N. C. 27711

April 1975

ia

This report is issued by the Environmental Protection Agency to report technical data of interest to a limited number of readers. Copies are available free of charge to Federal employees, current contractors and grantees, and nonprofit organizations - as supplies permit - from the Air Pollution Technical Information Center, Environmental Protection Agency, Research Triangle Park, North Carolina 27711; or for a fee, from the National Technical Information Service, 5285 Port Royal Road, Springfield, Virginia 22161.

This report was furnished to the Environmental Protection Agency by Flow Research, Inc., Kent, Washington 98031, in fulfillment of Contract No. 68-02-1294. The contents of this report are reproduced herein as received from Flow Research, Inc. The opinions, findings, and conclusions expressed are those of the author and not necessarily those of the Environmental Protection Agency. Mention of company or product names is not to be considered as an endorsement by the Environmental Protection Agency.

Publication No. EPA-450/3-75-066

Laboratory Simulation of Plume Dispersion from a Lead Smelter in Glover, Missouri: Neutral and Stable Atmosphere

by

Hsien-Ta Liu and Jung-Tai Lin
Flow Research, Inc., Kent, Washington 98031

Abstract

A series of laboratory experiments which simulated dispersion of pollutants from a lead smelter in Glover, Missouri were conducted in a stratified towing tank at Flow Research, Inc. Results of the experiments, including flow visualization records in the form of still and moving pictures and quantitative measurements with probes, were used here to determine the locations where high ground concentrations were most likely to occur under the simulated conditions.

In the laboratory, neutral and stable conditions corresponding to from typical to adverse cases observed in the atmosphere were produced. Four terrain models with a 1/2500 scale, simulating four wind directions, were constructed. Under neutral conditions, the plumes were considerably diluted within the simulated atmospheric boundary layer. Ground concentrations were low everywhere on the four models. Under stable conditions, the plumes were aloft upstream of the mountains, and ground concentrations were low. High ground concentrations were measured in some cases downstream of the mountains and at the locations where downslope winds occur. When the pollutants in the plumes were brought by the downslope wind into direct contact with the leeward mountain slope, the mean ground concentrations were high.

Based on the results of this study, one of the most unfavorable situations occurs when a strongly stable atmosphere is present. Therefore, it is recommended that samplers be installed on top of and downstream of the mountains.

Table of Contents

		Page
	Abstract	i
	Table of Contents	ii
	Nomenclature	iv
1.	Introduction	1
2.	Simulation Considerations	3
	2.1 Geometric Similarity	3
	2.2 Kinematic Similarity	3
	2.3 Dynamic Similarity	4
	2.4 Boundary Conditions	8
	2.5 Simulation Conditions	9
3.	Laboratory Facilities and Experimental Methods	11
	3.1 The Stratified Towing Tank	11
	3.2 Terrain Models	11
	3.3 Effluent Injection Device	12
	3.4 Flow Visualization Techniques	13
	3.5 Instrumentation	14
	3.5.1 Density Measurement	14
	3.5.2 Velocity Measurement	14
	3.5.3 Concentration Measurement	14
4.	Results of Flow Visualization	16
	4.1 Neutral Conditions	16
	4.2 Stable Conditions	17
	4.2.1 Stratification Effect	17
	4.2.2 Terrain Effect	18
5.	Probe Measurements	19
	5.1 Velocity Profiles	19
	5.1.1 Neutral, High-Wind Conditions	19
	5.1.2 Stable, Low-Wind Conditions	20
	5.2 Ground Concentration Measurements	21
	5.2.1 Neutral Conditions	21
	5.2.2 Stable Conditions	22
6.	Discussion and Recommendations	23
	6.1 Neutral, High-Wind Conditions	23
	6.2 Stable, Low-Wind Conditions	23
	6.3 Recommendations	23

TECHNICAL REPORT DATA
(Please read Instructions on the reverse before completing)

1. REPORT NO.	2.	3. RECIPIENT'S ACCESSION NO.
EPA-450/3-75-066		PB253437

4. TITLE AND SUBTITLE	5. REPORT DATE
Laboratory Simulation of Plume Dispersion From a Lead Smelter in Glover Missouri: Neutral and Stable Atmosphere	April 1975
	6. PERFORMING ORGANIZATION CODE
7. AUTHOR(S)	8. PERFORMING ORGANIZATION REPORT NO.
Hsien-Ta Liu and Jung-Tai Lin	Flow Research Report No. 55
9. PERFORMING ORGANIZATION NAME AND ADDRESS	10. PROGRAM ELEMENT NO.
Flow Research, Inc. 1819 S. Central Avenue Kent, WA 98031	2 AC 129
	11. CONTRACT/GRANT NO.
	68-02-1294
12. SPONSORING AGENCY NAME AND ADDRESS	13. TYPE OF REPORT AND PERIOD COVERED
Office of Air Quality Planning and Standards Environmental Protection Agency Research Triangle Park, NC 27711	FINAL May 1974 - Feb 1975
	14. SPONSORING AGENCY CODE

15. SUPPLEMENTARY NOTES

16. ABSTRACT

A series of laboratory experiments which simulated dispersion of pollutants from a lead smelter in Glover, Missouri were conducted in a stratified towing tank at Flow Research, Inc.. Results of the experiments, including flow visualization records in the form of still and moving pictures and quantitative measurements with probes, were used here to determine the locations where high ground concentrations were most likely to occur under the simulated conditions.

In the laboratory, neutral and stable conditions corresponding to from typical to adverse cases observed in the atmosphere were produced. Four terrain models with a 1/2500 scale, simulating four wind directions, were constructed. Under neutral conditions, the plumes were considerably diluted within the simulated atmospheric boundary layer. Ground concentrations were low everywhere on the four models. Under stable conditions, the plumes were aloft upstream of the mountains, and ground concentrations were low. High ground concentrations were measured in some cases downstream of the mountains and at the locations where downslope winds occur. When the pollutants in the plumes were brought by the downslope wind into direct contact with the leeward mountain slope, the mean ground concentrations were high. Based on the results, one of the most unfavorable situations occurs when a strongly stable atmosphere is present. Therefore, it is recommended that samplers be installed on top of and downstream of the mountains.

17. KEY WORDS AND DOCUMENT ANALYSIS

a. DESCRIPTORS	b. IDENTIFIERS/OPEN ENDED TERMS	c. COSATI Field/Group
Atmospheric diffusion		04A
Plumes		21B
Tests		14B
Stratification		14G
Terrain		08F

18. DISTRIBUTION STATEMENT	19. SECURITY CLASS *(This Report)*	21. NO. OF PAGES
RELEASE TO PUBLIC	UNCLASSIFIED	63
	20. SECURITY CLASS *(This page)*	22. PRICE
	UNCLASSIFIED	4.50

EPA Form 2220-1 (9-73)

Table of Contents (Cont'd)

		Page
7.	Conclusions	25
	7.1 Neutral, High-Wind Conditions	25
	7.2 Stable, Low-Wind Conditions	26
	References	28
	Tables	30
	Figures	33

Nomenclature

Symbol	Description	Dimension*
D	stack diameter	L
D_a	mass diffusivity of the ambient fluid	L^2T^{-1}
D_s	mass diffusivity of the stack effluent	L^2T^{-1}
d	diameter of the plume	L
F	buoyancy flux of the plume	L^4T^{-3}
F_D	stack Froude number, $\frac{W_s}{\sqrt{\frac{\Delta\rho}{\rho_s} gD}}$	-
F_H	internal Froude number based on the stack height, $\frac{U_\infty}{NH}$	-
f	frequency	T^{-1}
g	gravitational acceleration	LT^{-2}
H	stack height	L
h	characteristic height, such as that of a mountain	L
K	ratio of effluent velocity to free-stream velocity, $\frac{W_s}{U_\infty}$	-
κ_a	thermal diffusivity of the ambient fluid	L^2T^{-1}
κ_s	thermal diffusivity of the stack effluent	L^2T^{-1}
k	wave number	L^{-1}
k_K	Kolmogoroff wave number	L^{-1}
L	characteristic length	L
ℓ	geometric length	L
m	subscript referencing the model	-

*L = length, T = time, τ = temperature, M = mass

Nomenclature (Cont'd)

Symbol	Description	Dimension*
N	Brunt-Vaisala frequency, $\frac{1}{2\pi}\sqrt{\frac{g}{\rho_a}\frac{d\bar{\rho}}{dz}}$	T^{-1}
n	a constant	-
p	subscript referencing the prototype	-
R_D	stack Reynolds number, $\frac{W_s D}{\nu}$	-
R_h	Reynolds number based on the ridge height, $\frac{U_\infty h}{\nu}$	-
$S(f)$	one-dimensional energy spectrum function	L^2T^{-1}
s	stability parameter = $(2\pi N)^2$	T^{-2}
U	characteristic velocity	LT^{-1}
$\bar{U}$	mean velocity component in the x direction	LT^{-1}
$\bar{U}_i$	mean velocity in the i^{th} direction, i = 1, 2 and 3	LT^{-1}
U_∞	free-stream velocity	LT^{-1}
u	turbulent velocity	LT^{-1}
u_i	turbulent velocity in the i^{th} direction, i = 1, 2 and 3	LT^{-1}
u	velocity quantity	LT^{-1}
W_s	stack effluent velocity	LT^{-1}
x,y,z	Cartesian coordinate axes in longitudinal, lateral and vertical directions, respectively	L
Z	height of the plume trajectory above the stack exit	L
Z_t	height of the plume top above the stack exit	L
δ	turbulent boundary-layer thickness	L
θ	temperature deviation from the mean probe temperature	τ
$\bar{\theta}$	temperature	τ

Nomenclature (Cont'd)

Symbol	Description	Dimension*
$\overline{\theta}_s$	effluent temperature	T
ν_a	kinematic viscosity of the ambient fluid	L^2T^{-1}
ν_s	kinematic viscosity of the effluent	L^2T^{-1}
ρ_a	density of the ambient fluid at the stack-exit level	ML^{-3}
ρ_s	stack effluent density	ML^{-3}

1. Introduction

This report constitutes the primary results of a laboratory study that investigated, through physical modeling, plume dispersion from a lead smelter in Glover, Missouri under neutral and stable atmospheric conditions. The objective of this study was to determine the optimum locations for the installation of pollutant sampling stations in the vicinity of the prototype smelter. The experimental results also provided some of the data necessary for the validation of existing and future numerical models.

The stack under study is located at the American Smelting and Refining Company (ASARCO) sinter plant in Glover, Missouri. It is a custom smelter with an annual production capacity of 90,000 tons of lead. Effluent gases from the sinter machine, two clean-up conveyors, the sinter breaker, the spiked roll, the pan conveyor, and the cooling drum are vented through a water spray-chamber and a baghouse containing microtan synthetic bags. Before passing through the baghouse, exhaust gases are cooled by introducing ambient air through a vent. Then, the gases pass through the baghouse and are vented through a 186-m concrete stack that is 3.66 m in diameter (Shea, 1973).

The smelter is located approximately .5 km SW of Glover, Missouri in the valley of Big Creek. The surrounding terrain is quite rugged, being mostly rolling hills and small creek valleys. The whole area is heavily forested, with trees averaging from 5 to 10 m in height. Four mountains located approximately 4-6 km from the stack (see fig. 1), contribute further complexity to the terrain features. The four terrain models were constructed so that the plumes were advected toward these mountains.

The effects of complex terrain on plume dispersion have been investigated by Orgill, et al. (1971), Veenhuizen, et al. (1973) and Lin, et al. (1974). In particular, under stable conditions, Lin, et al. (1974) demonstrated that the plume dispersion phenomenon is complicated and that the associated pollution problems are localized. Most importantly, previous studies have demonstrated that many atmospheric flow phenomena in complex terrain under stable conditions can be accurately reproduced in a stratified towing tank (Lin, et al., 1974).

The present study investigated plume dispersion from the main stack under both neutral and stable atmospheric conditions. Laboratory experiments

using four 1/2500-scale terrain models which simulated four wind directions were undertaken in the Flow Research stratified towing tank. Flow visualization tests using a dyed plume were conducted. Quantitative measurements of ground concentrations were made with thermistor probes, and velocity profiles were measured with hot-film probes.

This report is divided into six sections. The simulation criteria and conditions are discussed in section 2. In section 3, the laboratory facilities and experimental methods used in this study are described. Results of flow visualization and of probe measurements are presented and discussed in sections 4 and 5, respectively. Further discussion and recommendations for the installation of full-scale pollutant samplers are presented in section 6. Finally, a few important conclusions derived from the study are summarized in section 7.

2. Simulation Considerations

In the simulation of flow phenomena in the laboratory, complete similarity between the model and the prototype can be achieved only if they are geometrically, kinematically, and dynamically similar (Sedov, 1959). For plume dispersion in stratified flows over complex terrain, simulation parameters can be derived, through dimension analysis, from physical variables which govern the flow field and the dispersion process (Lin, et al., 1974). In this section, simulation parameters and their physical interpretations that are relevant to this study are discussed.

2.1 Geometric Similarity

To satisfy the geometric similarity, the ratio of any geometric length ℓ to a characteristic length L of the model must be identical to that of the prototype; that is,

$$\left[\frac{\ell}{L}\right]_m = \left[\frac{\ell}{L}\right]_p, \tag{2.1}$$

where the subscripts m and p refer to the model and the prototype, respectively. In this study, the geometric scaling factor was selected to be 1/2500. The geometric length includes not only the sizes of the stack and the terrain features, but also the physical sizes of the flow field and the plume. For the flow field, the thickness of the atmospheric boundary layer and the sizes of the energy-containing eddies, which dominate the plume dispersion within the boundary layer, must be modeled according to the same scaling factor. For the plume, the plume trajectory, the width and height of the plume, and the terminal rise of the plume in a stratified flow must be scaled by the same factor.

2.2 Kinematic Similarity

Kinematic similarity requires the ratio of any velocity quantity u to a characteristic velocity U of the model to be identical to that of the prototype, namely,

$$\left[\frac{u}{U}\right]_m = \left[\frac{u}{U}\right]_p. \tag{2.2}$$

In reference to the plume, the speed ratio $\frac{W_s}{U_\infty}$, where W_s and U_∞ are, respectively, the effluent speed and the free-stream velocity, is the most important kinematic criterion to be reproduced in the laboratory. When simulating plume dispersion in the atmospheric boundary layer, however, one

must consider the reproduction of $\frac{\bar{U}_i}{U_\infty}$ and $\frac{\sqrt{\overline{u_i^2}}}{U_\infty}$, where $\bar{U}_i$ and $\sqrt{\overline{u_i^2}}$ are, respectively, the mean velocities and turbulence intensity in the i^{th} direction (i = 1, 2, and 3).

2.3 Dynamic Similarity

Once geometric and kinematic similarities are established, dynamic similarity requires the following criteria be satisfied:

(i) the stack Froude number similarity must be:

$$F_D = \left[\frac{W_s}{\sqrt{gD\,\frac{|\rho_s - \rho_a|}{\rho_s}}}\right]_m = \left[\frac{W_s}{\sqrt{gD\,\frac{|\rho_s - \rho_a|}{\rho_s}}}\right]_p , \qquad (2.3)$$

where F_D is the stack Froude number, g is the gravitational acceleration, D is the stack diameter, ρ_s is the effluent density, and ρ_a is the ambient fluid density;

(ii) the internal Froude number similarity must be:

$$F_H = \left[\frac{W_s}{NH}\right]_m = \left[\frac{W_s}{NH}\right]_p , \qquad (2.4)$$

where F_H is the internal Froude number based on the stack height H, and N is the Brunt-Vaisala frequency in Hz;

(iii) the stack Reynolds number similarity must be:

$$R_D = \left[\frac{W_s D}{\nu_s}\right]_m = \left[\frac{W_s D}{\nu_s}\right]_p , \qquad (2.5)$$

where R_D is the stack Reynolds number, and ν_s is the kinematic viscosity of the effluent;

(iv) the terrain Reynolds number similarity must be:

$$R_h = \left[\frac{U_\infty h}{\nu_a}\right]_m = \left[\frac{U_\infty h}{\nu_a}\right]_p , \qquad (2.6)$$

where R_h is the terrain Reynolds number based on the mountain peak height h, and ν_a is the kinematic viscosity of the ambient fluid;

(v) the ambient-fluid Peclet number similarity must be:

$$Pe_a = \left[\frac{U_\infty h}{\kappa_a}\right]_m = \left[\frac{U_\infty h}{\kappa_a}\right]_p ,$$

$$\text{or} \qquad Pe_a = \left[\frac{U_\infty h}{\nu_a}\right]_m \left[\frac{\nu_a}{\kappa_a}\right]_m = \left[\frac{U_\infty h}{\nu_a}\right]_p \left[\frac{\nu_a}{\kappa_a}\right]_p , \tag{2.7}$$

where Pe_a is the ambient Peclet number, $Pr_a = \nu_a/\kappa_a$ is the ambient Prandtl number and κ_a is the thermal diffusivity of the ambient fluid.

(vi) the stack Peclet number similarity must be:

$$Pe_s = \left[\frac{W_s D}{\kappa_s}\right]_m = \left[\frac{W_s D}{\kappa_s}\right]_p ,$$

$$\text{or} \qquad Pe_s = \left[\frac{W_s D}{\nu_s}\right]_m \left[\frac{\nu_s}{\kappa_s}\right]_m = \left[\frac{W_s D}{\nu_s}\right]_p \left[\frac{\nu_s}{\kappa_s}\right]_p , \tag{2.8a}$$

where Pe_s is the stack Peclet number, $Pr_s = \nu_s/\kappa_s$ is the Prandtl number and κ_s is the thermal diffusivity of the stack effluent.

(vii) the pollutant Peclet number similarity must be:

$$Pe_p = \left[\frac{W_s D}{\nu_s}\right]_m \left[\frac{\nu_s}{D_p}\right]_m = \left[\frac{W_s D}{\nu_s}\right]_p \left[\frac{\nu_s}{D_p}\right]_p , \tag{2.8b}$$

where Pe_p is the pollutant Peclet number, $Sc_s = \nu_s/D_p$ is the Schmidt number of the pollutant and D_p is the mass diffusivity of the pollutant.

The stack Froude number, which represents the ratio of the inertial force to the buoyant force of the effluent, is an important parameter in the simulation of the plume dispersion. For example, under neutral conditions, the plume rise Z is solely determined by the dimensionless parameters F_D and K, the stack diameter D, and the distance downstream of the stack x (Briggs, 1969; Lin, et al., 1974)

$$\frac{Z}{D} = 1.6\, K F_D^{-2/3} \left(\frac{x}{D}\right)^{2/3} \tag{2.9}$$

The internal Froude number, which represents the ratio of the inertial force to the buoyant force of the ambient fluid, affects the plume dispersion in two ways. First, the stratification inhibits the vertical rise of the plume. The terminal rise of the plume Z_t in a calm and stable fluid is governed by the stratification and the buoyancy flux of the plume, F (Briggs, 1969; Lin, et al., 1974), as

$$Z_t = 5F^{1/5}s^{-3/8} \quad . \tag{2.10}$$

Secondly, the stratified flow interacts with distinctive terrain features, such as mountains and valleys, which in turn govern the plume dispersion. For example, the formation of mountain lee waves, which considerably alter the flow patterns in the lee of a mountain, is governed by the internal Froude number (Turner, 1973). Therefore, the plume dispersion in a rugged terrain where lee waves are generated is also governed by the internal Froude number.

In the FRI towing tank, experimental conditions can readily be selected to match the stack Froude number and the internal Froude number usually encountered in the atmosphere. The similarities of the stack Reynolds number and the terrain Reynolds number, however, cannot be satisfied since the Reynolds numbers in the laboratory are about 3 to 4 orders of magnitude smaller than those in the field. The following discussions demonstrate that this lack of similarity between R_D and R_h does not seriously impair the validity of a realistic simulation.

Experimental data (Hoult and Weil, 1972 and Lin, et al., 1974) have shown that the plume rise, under neutral and stable conditions, is independent of the stack Reynolds number R_D as long as the plume is fully turbulent at the exit of the stack. A turbulent plume can be achieved by installing a tripping device a short distance upstream of the stack exit (see section 3.3). Remarkable correlation of the plume rise in calm and stable fluids has been obtained for plumes of vastly different sizes (section 4.2.1). Many investigators (e.g., Schlichting, 1968) have shown that flow phenomena are only weakly dependent on the Reynolds number R_h when R_h is sufficiently large and the flow is fully turbulent. Under neutral conditions, the region of most concern is the turbulent boundary layer (TBL), in which advection and mixing of pollutants in the plume occur. The turbulent motion must be simulated such that the turbulent energy and its distribution among the energy-

containing eddies, which effectively disperse the pollutants in the plume, are scaled according to the scaling factors of length and velocity. In the laboratory, atmospheric turbulent boundary layers can be realistically simulated (Plate, 1971). Various tripping methods have been successfully employed to provide a thick TBL with a realistic turbulent structure (Counihan, 1969; Yu and Lin, 1975). The TBL in this study was tripped, and the turbulent structure of this tripped TBL was in good agreement with field data (section 5).

Under stable conditions, however, the TBL is usually thin and the turbulent intensity in the TBL is usually low (Slade, 1969). Field observations (Schiermeier and Niemeyer, 1968, figs. 11 and 12) show that a plume released from a tall stack usually rises above the thin TBL and levels off in the form of a suspended thin ribbon in the laminar-like environment. Such behaviors of the plume have been realistically reproduced in a stratified towing tank (Lin, et al., 1974). The trajectories of the simulated plumes are in good agreement with field data (Briggs, 1969). The internal Froude number F_H is therefore more important than the terrain Reynolds number R_h in simulating plume dispersion under stable conditions. Over a complex terrain, the mean flow field is influenced by the stratification and the terrain features, or by definition, by the internal Froude number (based on the characteristic height of the terrain). In a laminar-like flow region, the plume dispersion is mainly governed by the mean flow field and, therefore, by the internal Froude number.

The similarities of the Peclet numbers described in eqs. (2.7) and (2.8) are discussed in the following. In the case where the same fluid is used in the laboratory and in the field, similarity of the ambient Peclet number and the stack Peclet number cannot be satisfied because the Peclet numbers in the laboratory are approximately three to four orders of magnitude smaller than those in the field. Hence, following the argument on the similarity of the Reynolds number, the similarity of the Peclet number is not critical if the flow is turbulent. For the present investigation, salt water was the working fluid. Because the Schmidt number $Sc_a = \nu_a/D_a$ or $Sc_s = \nu_s/D_s$ of salt water has a value of approximately 700 and because the Prandtl number of air for the field situation is about 0.7, the Peclet number in the laboratory is the same order of magnitude as that in the field. The advantage of using salt water instead of air as the working medium is therefore quite clear. Note that this argument is valid

for the motion of energy-containing eddies, which is our basic concern here. This argument is not valid, however, for the motions of small-scale eddies, which have a scale of approximately the order of the Kolmogorov length (Hinze, 1959) because the spectrum contains a k^{-1} region for the scalar quantity of a high Schmidt or Prandtl number but not for those of a low Schmidt or Prandtl number.

The similarity of the pollutant Peclet number requires further consideration. To simulate the pollutant concentration for the present study, we used the temperature excess of a heated plume as the tracer. Because the Prandtl number of water is about 7 and the Schmidt number of the pollutant in the field is approximately the order of unity, we therefore estimate the pollutant Peclet number in the laboratory to be about two or three orders of magnitude smaller than that in the field. Two conditions are considered concerning the similarity of the pollutant Peclet number. First, in a neutral atmosphere, the boundary layer flow over the terrain is turbulent, and thus, the plume dispersion is governed by the turbulent motion in the TBL and in the plume. Therefore, we can follow the argument for the Reynolds number and expect that the Peclet number does not need to be critically simulated. Secondly, in an extremely stable atmosphere, the background flow is laminar-like, but the plume in the laboratory remains turbulent for about 2000 diameters downstream of the stack. For the present study, the plumes traveled less than 2000 diameters (7.2 km) downstream of the stack before they were broken up by the downslope wind (section 4.2). Again, in the turbulent region of the plume, the similarity of the Peclet number is not a critical requirement.

2.4 Boundary Conditions

The laboratory simulation was conducted in a towing tank (section 3.1). The side and bottom walls of the tank could impose some effects on the plume dispersion. For the present study, the maximum plume spread was about 30 cm in width and depth, which is only one-third of the tank width and depth. Therefore, the effects of the side walls were expected to be insignificant. To simulate an absorptive upper boundary for the stable cases, layers of nylon netting were installed on the bottom of the tank because the model was towed upside down.

The boundary conditions on the terrain model surface are the nonslip of the velocity and the nontransport of heat and mass through the surface.

The latter condition was maintained by the use of polyurethane foams, an insulation material, to construct the terrain models.

2.5 Simulation Conditions

As stated in section 1, the primary objective of the present investigation was to determine, through laboratory simulation, the optimum locations for the installation of air-quality sampling stations at the Glover site. In designing the experiment, one of the critical steps was to select a length scale according to the capacity of the laboratory facility such that the above-mentioned similarities were satisfied. As shown in the contour map of the vicinity surrounding the Glover ASARCO plant (fig. 1), the area of interest is about 12 km x 8 km. The towing tank used for the experiment has a width of 1.2 m, and thus, if the entire area of interest were modeled, a scaling factor of 1/10,000 would be required. With this scaling factor, the stack model would have a height of about 2 cm and an exit diameter of about 0.4 mm, and the Ketcherside Mountain, which is the highest mountain in this area, would be about 5 cm high. According to previous experiments (Veenhuizen, et al., 1973), the diameter of this stack model is probably too small to produce a turbulent plume at the stack exit; and therefore, if a turbulent plume is desired, the stack diameter ought to be exaggerated; this would violate the geometrical similarity and is undesirable. Instead of modeling the entire 12 km x 8 km area, four separate terrain models (1/2500 scale), which correspond to the four rectangular areas marked in fig. 1, were constructed to simulate four wind directions. In each wind direction, one of the four major mountains is located directly downstream of the stack. It was speculated that the ground concentrations in the vicinity of the mountains would be high under these simulated wind directions.

The present investigation attempted to simulate both neutral, high-wind and stable, low-wind conditions in the Flow Research stratified towing tank. The physical data and the effluents for the main stack of the Glover ASARCO plant were provided by the Environmental Protection Agency, Research Triangle Park, North Carolina, and they are listed in table 1. Also, the atmospheric conditions, such as the wind speed and the lapse rate, which are expected to be from typical to extreme in the area of Glover, Missouri, are provided and tabulated in table 2.

The dimensionless parameters K, F_H and F_D calculated for the field case were reproduced in our experiments. For all experiments, we selected the scaling factor of length to be 1/2500. Under neutral conditions, we selected the scaling factor of velocity to be 1/64, and therefore, the scaling factor of time was 1/40. In other words, the flow phenomenon observed for one second in those experiments has the corresponding time scale of 40 seconds in the full-scale case. Under stable conditions, the scaling factor of velocity was 1/83, and therefore, the scaling factor of time was 1/30.

3. Laboratory Facilities and Experimental Methods

3.1 The Stratified Towing Tank

Experiments were performed in a stratified towing tank, 18.3 m long, 1.2 m wide and .9 m deep. A detailed description of this facility has been given in a previous FRI report (Pao, et al., 1971). Special features of the towing tank system that are pertinent to the present investigation are described briefly in the following: (1) It has a specially designed filling system, which facilitates the preparation of a stratified fluid with any desired stable stratification. (2) It has a smooth, oil-lubricated carriage with a noise level that is approximately 0.6% of the towing speed. These features allow accurate measurements of the velocity, temperature, and salinity fluctuations with hot-film probes, thin-film and/or thermistor probes, and single-electrode, conductivity probes. (3) It has transparent side and bottom walls, which allow flow visualization experiments from several directions. (4) It has a minicomputer system for direct on-line multiple-channel data acquisition and subsequent statistical data analysis.

3.2 Terrain Models

Four terrain models of 1/2500 scale were constructed to simulate four wind directions (see fig. 1). First, enlarged prints of 1/2500 scale were made photographically on mylar sheets (Technical Service Department, the Boeing Company) from the USGS 7½-minute topographic maps. The models, 3.7 m long and 1.1 m wide, were made of polyurethane foams (approximately 9.6 Kg/m^3), according to the enlarged mylar contour maps, with a router. The model surfaces were intentionally constructed to be stepped with vertical increments of .24 cm corresponding to 6.1-m contour intervals in the prototype. The stepwise feature of the model realistically represents the roughness condition of the prototype terrain, on which trees from 5 m to 10 m in height were forested. A 4.9-m-long platform, made of a 1-cm-thick acrylic sheet reinforced with aluminum angles, was built to support the terrain models. It was designed so that individual terrain models could be interchanged with each other in the towing tank. Two-dimensional fences made of .3-cm acrylic sheets, with a maximum-height of 2 cm and a spacing of 2.5 cm, were installed in the upstream 1.3-m portion of the platform to serve as a turbulent-boundary-layer tripping device. The fences were also designed to conform with the general features of the prototype terrain.

The most pronounced features of Model I, the Vickery Mountain (elev. 488 m) and the valleys of Carver Creek and of Big Creek, are primarily two-dimensional (fig. 1). The Vickery Mountain spans almost the entire width of the model. The terrain features of Models II and III are essentially three-dimensional. The horseshoe-shaped Hogan Mountain (elev. 512 m) in Model II is situated such that the vertical cross-section along the centerline of the model shows two humps. The Ketcherside Mountain (elev. 518 m) in Model III has a single peak and is the highest of the four mountains. The valley of Big Creek extends over both models II and III and makes a small angle with the centerlines of the models. Model IV has features similar to those of Model I, with another mountain (no name) and the valley of Big Creek as the outstanding landmarks. The mountain (elev. 485 m), which is about the same size as the Vickery Mountain, also spans a large portion of the model width. Figure 2 shows enlarged contour maps of the individual models. In these maps, the stack, denoted by a solid circle, is located on the right-hand side. The locations of the thermistor probes used for the pollutant measurement are indicated by solid stars, and the numbers nearby denote the probe numbers.

During the experiment, terrain models and the stack were mounted upside down on an oil-lubricated carriage in the stratified towing tank. To simulate a buoyant plume in the atmosphere, a heavy plume was injected from an inverted stack into the ambient fluid.

3.3 Effluent Injection Device

A concentrated dye solution (brilliant-blue food dye) with $\rho_s = 1.17$ $\left|\text{Kgfs}^2\text{m}^4\right|$ was used as the effluent. The injection device consisted of a heated flask containing the effluent fluid, a temperature controller (YSI Model 72), a veristaltic pump (Manostat Model 72-895-05) using insulated tygon tubing, an accumulator, and a heated hose (Technical Heaters, Inc., Model 352) connected to the stack. First, the dye solution was preheated to 80°C in the flask. The dye solution was then pumped through the heated hose, where the temperature was controlled at $90 \pm 2^{\circ}$C, and finally, it was forced out the stack into the ambient fluid. The heat contained in the plume served as a tracer, and the ground concentrations were then measured with thermistor probes. Because a low concentration level was expected, the variation of the temperature of the fluid in the towing tank had to be small. To maintain the temperature variation along the tank to within $\pm.01^{\circ}$C, the side walls of the tank and the water surface were insulated with sheets of polyurethane foam, and a grid with vertical

rods (1.3 cm in diameter) was towed in the tank at least one hour before each experiment. For a heated plume at 90°C and the ambient fluid at 20°C, the thermal noise level $(\theta - \theta_a)/(\theta_s - \theta_a)$, corresponding to .01°C, was therefore 1.4×10^{-4}.

The injection device included a tripping device that ensured the plume was turbulent at the stack exit. This tripping device was made of a sapphire nozzle, .018 cm in diameter, which was installed about .5 cm upstream of the stack exit. For an untripped plume, the flow was laminar when the stack Reynolds number was about 200. When the plume was tripped, the Reynolds number at the nozzle was increased to about 1600, which is much higher than the critical Reynolds number. The distance between the nozzle and the exit of the stack was found to be critical. If the distance was smaller than required, the flow at the stack exit would be governed by the nozzle instead of the stack. On the other hand, if the distance was significantly larger than required, the flow tripped by the nozzle would relaminarize before it reached the stack exit. After a series of tests, a distance of 0.5 cm between the nozzle and the stack exit was found to be satisfactory.

3.4 Flow Visualization Techniques

The tracer effluent used in the experiments was a mixture of salt water and a brilliant-blue food dye. The plume was photographed with still and movie cameras, as follows:

- One 35-mm still picture camera was towed with the terrain model to record the side view of the plume, and one 35-mm still picture camera stationary to the tank was used to record the plan view.
- Two 16-mm movie cameras were towed to record the side and angle views.
- Two 35-mm still picture cameras carried by photographers were used to record plume dispersion from various angles.

The back diffusive lighting, used for flow visualization, was provided by three fluorescent light panels, each of which was 61 cm wide and 122 cm long, suspended from the towed carriage. The light was diffused by inserting translucent, acrylic sheets, which were .32 cm thick and transmitted 53% of the incident light, between the light panels and the towing tank. The visualization records have been summarized in still pictures and in a movie film (Liu, et al., 1975), which constitutes an essential portion of the final report.

3.5 Instrumentation

3.5.1 Density Measurement

A conductivity gauge (Model 1010) manufactured by Flow Research, Inc., was used to measure the density profile in the tank. This gauge has a frequency response from DC to 1 KHz. The sensor was a single-electrode conductivity probe, which was a .025-mm stainless-steel tip platinized with platinum black solution. The sensitivity of the conductivity gauge was about 1 volt per 0.025 gm/cm^3. The probe was calibrated in jars of salt solution of known density. Then, the calibration data were least-square fitted with a second-degree polynomial. Figure 3 is a typical density profile (Run IVb) measured in the towing tank. The Brunt-Vaisala frequencies calculated from the density profiles for individual runs are tabulated in table 2.

3.5.2 Velocity Measurement

The mean and turbulent velocities of the incoming flow near the stack were measured with two 10-channel constant-temperature anemometers (1053-B, Thermo-Systems, Inc.) and thirteen conical, and one cylindrical, hot-film sensors (TSI Models 1230S and 1290 AK). For use in salt water, the sensors are coated with quartz. The anemometer has a frequency response of up to 1000 Hz. The hot-film sensors were mounted on a vertical strut covering a vertical distance of 30 cm, with the spacing between sensors decreasing toward the terrain surface. The vertical strut and the terrain model were towed with the same carriage system. For calibration, the strut was moved to a distance of about 30 cm lower than the position during the velocity measurement. This allowed the probes to be free from disturbances induced by the terrain model. This arrangement introduced, however, a small error in measuring velocity in a stratified fluid because the probes were not calibrated in the same fluid as that in which the measurement was conducted. For the experiments conducted, the fluid density varies by a factor of 3% for a vertical distance of 30 cm, and by referring to the appendix described in Flow Research Report 57 (Liu and Lin, 1975), we estimated the errors involved in the measurements of the mean and turbulent velocity to be about 5% and 4%, respectively. Note, however, that this type of error would not occur for the case of a non-stratified fluid.

3.5.3 Concentration Measurement

Using temperature as a tracer, we measured ground concentrations with thermistor probes (Fenwal Electronics GC32SM2). The thermistor probes have a

nominal resistance of 2000Ω and a temperature coefficient of -3.4%/^{o}C at room temperature. The probe tip is 0.076 cm in diameter, and the time constant (3db point) of the thermistor probe in still water is about .07 sec. A 10-channel gauge with the thermistor probe as one arm of the wheatstone bridge was used to measure temperature in the fluid. The sensitivity of the system is typically 10 V/^{o}C, and the noise level is about 3 mV peak-to-peak. The thermistor probe has a long-term stability, and a typical drift is .01^{o}C/year.

The probes were first calibrated against a precision thermometer with an accuracy of .01^{o}C (Brooklyn Thermometer Company, Inc.) in a constant-temperature bath which was equipped with a temperature controller (YSI Model 72) with an accuracy of .01^{o}C. In the range of temperature differences of interest (0 ~ .5^{o}C), the pre-calibration curves appear to be linear (fig. 4). To obtain the in-situ calibrations for the probe located in the tank, we followed the procedure described below. First, the temperature of the fluid in the tank and the voltage output of the thermistor probe were measured. These measurements provided one data point for the in-situ calibration, and the curve was then obtained by extrapolating this data point using the known slope of the pre-calibrated curve. For ground concentration measurements, the probe tips were located about 2 mm above the surface of the terrain model. The locations of the probes, in reference to the stack, are indicated by solid stars in fig. 2.

4. Results of Flow Visualization

The visualization results are illustrated in still pictures (figs. 5 through 8) and are discussed in this section. In addition, a 16-mm color film (Liu, et al., 1975) containing the essential visualization results is included as an important supplement to the report. Frequent reference to this movie is made in this context to aid in interpretation of the results.

Figures 5 through 8 are photographs that show the side and plan views of the dispersing plume over the terrain models. The plan views were photographed with a camera that was stationary to the towing tank. These photographs show the evolution of a section of the plume with time as the models were towed by. An overall picture of the plume on the horizontal plane was obtained by splicing the slightly overlapping frames together in sequence. The side view of the plume was photographed through the viewing sections of the towing tank with a camera mounted on the carriage and towed along with the individual models. These photographs not only provide the overall picture of the plume, but also help interpret the ground concentration measurements by pinpointing the regions of high ground concentrations.

4.1 Neutral Conditions

Under neutral conditions, a simulated turbulent boundary layer was generated for all the terrain models. The side views of the plume dispersion are seen in figs. 5a, 6a, 7a and 8a. In the near region, say within a few hundred stack-diameters downstream of the stack, the plume trajectory appears to fluctuate with time, in contrast with that observed in a laminar background flow. Farther downstream, the plume is broken up and no coherent trajectory is observed. The plume disperses in a patchy manner; this dispersion pattern indicates the motion of large eddies in the boundary layer. Occasional touchdown of pollutant "pockets" on the ground was observed for short periods. The ground concentrations, however, are expected to be low since pollutants are diluted considerably inside the turbulent boundary layer. The plan views of the plume (figs. 5c, 6d, 7d and 8d) show that the plume axes are nearly parallel to the wind direction and that the local topography does not cause any appreciable distortion of the plume axes.

The TBL's over the terrain models were tripped to render realistic simulation of the atmospheric boundary layer in which plume dispersion is studied. The characteristics of the tripped TBL are discussed in section 5.1.

To emphasize the importance of establishing a realistically simulated TBL when modeling plume dispersion under neutral conditions, fig. 9 shows a side view of the plume in Run IVa. This view was photographed shortly after the terrain model was towed and after it had reached a constant speed, but before the TBL was fully developed. Note that the only mixing of the plume was introduced by the turbulent motion inside the plume. The striking difference between fig. 8a and fig. 9 is evident.

4.2 Stable Conditions

Under stable, low-wind conditions, the plumes over individual models display many interesting features, several of which are common to all models and others which are distinctively unique. These differences indicate that the interaction of stratified flows and topography appears to significantly influence the flow field in the vicinity of the terrain, which in turn affects the dispersion patterns of the plume. Two stability conditions, which correspond to typical cases observed in the atmosphere, were simulated for each model except Model I (see table 2).

4.2.1 Stratification Effect

As shown in figs. 5 through 8, a plume over complex terrain under stable conditions is markedly different from a plume under neutral conditions. Under stable conditions, both the rise and the vertical spread of the plume are limited. For small internal Froude numbers, overshooting of the plume from its terminal height is noticeable. The striking resemblence among the plumes shown in figs. 5 through 8 and the TVA Keystone plume under a stable atmosphere (Schiermeier and Niemeyer, 1968) indicate that the simulation is indeed realistic. Note that the same TBL tripping device used in the neutral cases was employed in the stable cases. Apparently, the mechanical turbulence generated by the tripping device and the downstream rugged terrain surface is considerably damped by stratification. The well-defined plume edges indicate that the turbulence intensity at the plume level is very low. This observation coincides with field data (Slade, 1969), which show that the TBL in a stable atmosphere is thin and has a low turbulence intensity. The top of the plumes for the low Froude-number cases are measured from the side views of the plumes, and the results are plotted vs. $5F^{1/4}s^{-3/8}$ in fig. 10. Other results available from Briggs (1969) and laboratory measurements by Lin, et al. (1974) are also plotted. The empirical equation, expressed in eq. (2.10) and drawn as a solid line in

fig. 10, correlates all the data very well. This finding shows that, despite the low stack ($R_D \sim 200$, untripped) Reynolds number encountered in the present investigation, the plume has been successfully tripped to be turbulent, and the plume dispersion has been properly simulated.

4.2.2 Terrain Effect

Upstream of the mountains, the plumes are aloft, and the terrain effect on plume dispersion is insignificant, except for the case, $F_H = 5.4$, shown in fig. 6b. The shape of the plume in fig. 6b appears to conform closely to the two humps of the Hogan Mountain. This, the only observed terrain effect, lessens considerably as the internal Fourde number is reduced by a factor of two ($F_H = 2.7$), as shown in fig. 6c. Concerning the lateral spreading, no significant meandering is observed for any of the four models.

The terrain effect on plume dispersion is, however, observed just downstream of the mountaintops. There is strong downslope wind downstream of the mountaintops, and this flow carries the plume toward the leeward mountain slope. In all the visualization results, only the plumes shown in figs. 5b and 7c could have direct contact with the leeward mountain slopes. Figure 5b corresponds to Run Ib, which has the lowest internal Froude number ($F_H = 2.2$), and fig. 7c corresponds to Run IIIc ($F_H = 2.7$), which has the highest mountain of all the four models.

As the downslope wind carries the plume closer to the leeward mountain slope, the terrain effect on plume dispersion becomes stronger. The plumes shown in figs. 7f, 8e and 8f tend to divert from the ambient wind direction. Closer examination of the terrain features indicates that the plume is either carried around the mountain peak (fig. 7f) or is forced to follow a valley along the leeward mountain slope (figs. 8e and 8f). When the plume is aloft, however, no appreciable meandering is observed, and the plume axis is parallel to the ambient wind direction (fig. 7e).

The generation of lee waves is demonstrated by several traces of the plumes, which are shown in figs. 6b, 6c, 8b and 8c. The wavelength of the lee waves traced by the plumes decreases as the internal Froude number decreases. The vertical spread of the plume appears to thicken downstream of the first wave trough (figs. 6b and 8b). For a few low internal-Froude-number cases (figs. 6c, 7c and 8c), the waves are actually broken up. The lateral spreads (figs. 5a and 7f) corresponding to the low internal-Froude-number cases ($F_H = 2.2$ and 2.7, respectively) tend to increase abruptly at locations where the waves are broken up, and therefore, a strong turbulent region is indicated.

5. Probe Measurements

5.1 Velocity Profiles

5.1.1 Neutral, High Wind Conditions

The vertical profiles of mean and turbulent velocities were measured in the vicinity of the stack for the four terrain models. The profiles provided the basic information on the turbulent motion in the boundary layer. The results are presented in figs. 11a through 11d. In these figures, the origin of the coordinate system (x,y,z) refers to the coordinates of the stack base. For all the four runs, the towing speed of the terrain model or the free-stream velocity U_∞ was 12.6 cm/sec. The thickness of the boundary layer δ, defined as the vertical distance at which the mean velocity $\overline{U}$ is equal to $0.99U_\infty$, ranges from 22 cm to 27 cm for the four models.

The mean velocity profiles are replotted as $\overline{U}/U_\infty$ vs. z/δ in fig. 12. For a major portion of the profile, the mean velocity can be approximated by a power law

$$\frac{\overline{U}}{U_\infty} = \left(\frac{z}{\delta}\right)^{1/n}. \tag{5.1}$$

The mean value of n for the four models is about 3. It has been reported that $n = 7$ for turbulent flows over a smooth or rough flat plate (Schlichting, 1968) and $n \approx 6$ to 4 for flows over wind-generated water waves (Liu and Karaki, 1973). The smaller value of n for the present case is believed to result from the rugged surface boundary; Plate (1971) has shown that the value of n tends to decrease with an increase in surface roughness.

The vertical profile of the longitudinal turbulent velocity shown in figs. 11a through 11d is also different from the profile of the turbulent velocity observed in a turbulent boundary layer over a smooth or rough plate (Hinze, 1959). For the present case, the profile appears to have a thick region $z/\delta < 0.5$, in which the turbulent intensity is as high as 10 to 12% of the free-stream velocity. Note that, in the experiments, the plume was released at a level $z = 7.4$ cm, and its trajectory was influenced by the turbulent motion even in the region immediately downstream of the stack (figs. 5a, 6a, 7a and 8a).

Further examination of the characteristics of the turbulent boundary layer is possible from the measurement of the one-dimensional energy spectrum.

Figure 13 shows the turbulent spectra $S(f)$ calculated from the measurement of the longitudinal turbulent velocity for Run IIIa. Here, f is the frequency in Hz, and $S(f)$ is in $cm^2/sec^2/Hz$. The first two sets of data, indicated by circles and crosses, were measured within the turbulent boundary layer at $z = 1.2$ and 7.8 cm, respectively. The third set of data, indicated by triangles, was measured outside the turbulent boundary layer at $z = 29.6$ cm, and therefore, it can be considered the noise spectrum when examining the turbulent spectrum. In the frequency range where most of the turbulent energy is contained, the turbulent spectrum is about two decades above the noise spectrum.

The turbulent spectrum measured at $z = 7.8$ cm is replotted in fig. 14 as $fS(f)/\overline{u^2}$ vs. k, where k is the wave number in cycle/m. The energy peak appears at about $k \approx 3$ cycle/m or at a length scale of about 33 cm, which is comparable to the thickness of the boundary layer. For comparison, the field data, compiled by Davenport (1961) and available from Lumley and Panofsky (1964), are plotted in fig. 14. The size of turbulent eddies measured in present experiments is scaled upward by a factor of 2500 because the model scale was 1/2500. In the range of the energy-containing eddies, the scaled-up laboratory result is in good agreement with the field result. This finding indicates that the energy-containing eddies in the atmosphere can be scaled down and simulated with proper energy contents. This result also indirectly shows that the plume dispersion in the atmospheric boundary layer can be simulated in the laboratory as long as the plume dispersion is dominated by the turbulent motion of energy-containing eddies.

5.1.2 Stable, Low-Wind Conditions

In these experiments, identical terrain models and tripping mechanisms, as described in section 3.2, were used. The vertical profiles of the mean velocity for the internal Froude number $F_H = 2.7$ and 5.4 are plotted in figs. 15 and 16, respectively. Comparison of fig. 11 with figs. 15 and 16 shows marked differences in the mean velocity profiles under neutral and stable conditions, as the result of the interaction of the stratified flow and the rugged terrain. The most obvious differences are the appearance of the overshooting and the large wind shear observed in figs. 15 and 16.

The turbulent velocity $\sqrt{\overline{u^2}}$ is relatively low, and its distribution is scattered. Adjacent to the terrain surface in a thin layer, (<6 cm), $\sqrt{\overline{u^2}}/U_\infty$ is about 4 to 8% while, at the plume level, $\sqrt{\overline{u^2}}/U_\infty$ is practically zero.

The mechanical turbulence generated by the rough terrain tends to be rapidly damped by the stable stratification. The TBL is confined only in a thin layer, above which any disturbance is damped.

5.2 Ground Concentration Measurements

The temperature in the heated plume was used to indicate the pollutant concentration. For ground concentration measurements, 10 thermistor probes were installed 2 mm above the terrain surface in each model where high concentrations were likely to occur. The locations of the probes (fig. 2) were designed for both neutral and stable conditions. Those probes installed upstream of the mountains were primarily for the neutral conditions, but also provided records of the ambient temperature for the stable conditions.

5.2.1 Neutral Conditions

For all four models tested, we did not observe any measurable concentration at the ground because the signals detected by the thermistor probes are indistinguishable from the thermal noise ($\sim 0.01^{\circ}$C in the towing tank). For the effluent at a temperature of 90°C and the ambient fluid at 20°C, the resolution in measuring the pollutant concentration level is 1.4×10^{-4} in a dimensionless unit. A simple argument is given in the following to demonstrate the low level of concentration possible for a plume dispersed in a turbulent boundary layer. The heat flux released from the stack is calculated by

$$Q = \frac{\pi}{4} D^2 W_s (\overline{\theta}_s - \overline{\theta}_a), \qquad (5.2)$$

where θ_s is the effluent temperature and θ_a is the ambient temperature. For the plume downstream of the stack, the pollutant is assumed to be distributed uniformly in a circular cross section of diameter d. The convection speed of the effluent is simply assumed to be the free-stream speed U_∞. Based on the conservation of heat (or pollutant) flux, the concentration level is calculated to be

$$\frac{\overline{\theta} - \overline{\theta}_a}{\overline{\theta}_s - \overline{\theta}_a} = \left(\frac{D}{d}\right)^2 \frac{W_s}{U_\infty} \quad . \qquad (5.3)$$

From the photographs shown in figs. 5a, 6a, 7a and 8a, the diameter d of the plume in the boundary layer is estimated to be about 20 cm for the region where the plume touches the ground. By inserting the values $D = 0.14$ cm

and $W_s/U_\infty = 1.4$, the concentration level is estimated to be

$$\frac{\overline{\theta} - \overline{\theta}_s}{\overline{\theta}_s - \overline{\theta}_a} = 0.7 \times 10^{-4},$$

which is even lower than the thermal noise level encountered in the towing tank.

5.2.2 Stable Conditions

As observed in the visualization results, the plumes are far above the ground in the upstream of the mountains. Low ground concentrations in this region are expected. Also, the visualization results show that the plumes are carried close to the ground on the top and lee sides of the mountains, and therefore, high ground concentrations are expected for the area around the mountains. Among the seven runs, only three of them (Runs Ib, IIIb and IIIc) show measurable ground concentrations. For the other cases, no detectable signal was observed.

In table 3, the results of temperature measurements are listed for Runs Ib, IIIb, and IIIc. The thermistor probes were numbered, and their locations downwind of the stack for the respective models are listed in the table. For Run Ib, the maximum ground concentrations were detected on the leeward side of Vickery Mountain (probes 7 and 8), where the downslope wind occurs, and on the mountain top (probes 4 and 5). The maximum root-mean-square (rms) concentrations, however, were detected farther downstream, where the plume tends to be mixed intensively (fig. 5b). In Run IIIb, the maximum mean and rms ground concentrations were detected simultaneously at locations (probes 9 and 10) downstream of the leeward mountain slope. For Run IIIc, the internal Froude number was reduced from 5.4 to 2.7, and the results are similar to those of Run IIIb. In Run IIIc, the downslope wind carries the plume closer to the leeward surface of the mountain (fig. 7c) than in Run IIIb (fig. 6b), and it also carries the plume around the top of Ketcherside Mountain (fig. 7f). As a result, the plume partially avoids probes 2 and 3; otherwise, the mean concentrations measured at probes 2 and 3 for Run IIIc would have been much higher than those shown.

6. Discussion and Recommendations

In the previous sections, results of the flow visualization have been presented to provide an overall view of plume dispersion in a complex terrain. Also, the measurements of velocity profiles and ground concentrations provided some quantitative understanding of the dispersion of pollutants. In this section, we shall further examine these results, and their implications for the field situation will be discussed. In the following discussion, we first assume that the effluent concentration of SO_2 at the stack exit is 2000 ppm in the field, and then, the ground concentration in the field is calculated based on the laboratory measurements.

6.1 Neutral, High-Wind Conditions

Under neutrally stable conditions, we did not detect any measurable concentration of pollutant. A simple argument, based on the conservation of the pollutant flux, was given in section 5.1 to show that the pollutant is so diluted that its concentration is lower than the thermal noise level, $.01^{\circ}C$, or in a dimensionless form, 1.4×10^{-4}, in the towing tank. This noise level corresponds to a full-scale background concentration of .28 ppm, which is lower than the Federal Ambient Air Quality Secondary Standard for SO_2 of .5 ppm for a 3-hour average. Note that the sampling time in the experiment for the attainment of ground concentrations ranged from 40 to 60 seconds, which corresponds to about 30 minutes in the full-scale case since the scaling factor of time is 1/40. We therefore conclude that the ground concentrations are unlikely to be higher than the SO_2 secondary standard of .5 ppm under the simulated neutrally stable atmosphere.

6.2 Stable, Low-Wind Conditions

We have measured significant ground concentrations in the area around the mountain for Runs Ib, IIIb and IIIc. For example, a concentration level as high as 2×10^{-3} was measured in the leeward side of the Ketcherside Mountain. The corresponding concentration of SO_2 in the field would be 4 ppm, which is much higher than the secondary standard. Note that the sampling time used to obtain the mean concentration level was about 40 seconds, which corresponds to 20 minutes in the field case since the scaling factor of time is 1/30.

6.3 Recommendations

Based on the results of this laboratory simulation, we recommend the following locations for the installation of pollutant samplers:

(1) Install samplers in the vicinity of Vickery Mountain. The sampling area should cover the range from $x = 4$ to 7 km directly downstream of the stack (figs. 5b and 5d).

(2) Install samplers in the vicinity of Ketcherside Mountain. The sampling area should cover the area from $x = 4$ to 7 km downstream of the stack along the centerline (with reference to the stack) of the model (figs. 7b and 7e) and about .5 km east of the centerline (figs. 7c and 7f).

(3) In the areas of Hogan Mountain and the unnamed mountain in model IV, we suggest to install some samplers although we did not detect any measurable ground concentration for the atmospheric conditions tested. When an elevated inversion layer occurs at a level about the same height of the mountain, high ground concentrations are expected. In the vicinity of Hogan Mountain, the sampling area should cover the range from 3 to 7 km directly downstream of the stack. In the vicinity of the unnamed mountain in model IV, the sampling area should cover from 4 to 7 km downstream of the stack. The samplers should be installed along the valley in the lee of the mountain, as indicated by the plume (figs. 8e and 8f).

7. Conclusions

From the results of flow visualization and of quantitative measurements with probes, we make the following conclusions.

7.1 Neutral, High-Wind Conditions

(i) Velocity profiles of the tripped turbulent boundary layer (TBL) at the stack location compare well with other flows over rough surfaces. A major portion of the vertical profiles of mean velocity, measured at the vicinity of the stack, can be approximated by the power law,

$$\frac{\bar{U}}{U_\infty} = \left(\frac{z}{\delta}\right)^{1/3}.$$

For the four models, the tripped boundary layer thicknesses are about 600 m, which is approximately three times the stack height. The profile of the longitudinal turbulent velocity over a complex terrain model contains a thick region, about 1/3 to 1/2 of the boundary layer thickness, in which the turbulent intensity $\sqrt{\overline{u^2}}$ has a value of about 10 to 12% of the free-stream velocity.

(ii) The energy spectrum of the longitudinal turbulent velocity fluctuation measured in the TBL is in good agreement with field data compiled by Davenport (1961). This agreement is important evidence that the atmospheric boundary layer and the associated pollutant transport can be realistically simulated in a towing tank.

(iii) The dyed plume released into the TBL shows that the turbulent motion of the TBL affects the plume dispersion even in the region very near the stack. The plume trajectory fluctuates, in contrast to the plume trajectory observed in a laminar background flow. Farther downstream, the plume is broken up and shows no coherent trajectory. The patchy formation of the plume indicates the existence of large eddies in the TBL.

(iv) The stack is relatively tall, compared with the surrounding topography. Apparently, the plume axes remain aloft throughout the entire lengths of the models (up to 7 km from the stack). In the area modeled, the maximum concentration at a given downstream distance does not occur on the ground.

(v) The temperature data shows that the ground concentrations are comparable to the thermal noise level, $.01^{\circ}C$ (or 1.4×10^{-4} in a

dimensionless unit) in the towing tank. This corresponds to a full-scale background concentration of .28 ppm (if a source concentration of 2000 ppm is assumed), which is lower than the SO_2 secondary standard of .5 ppm for a 3-hour average.

7.2 Stable, Low-Wind Conditions

(i) Velocity data show the presence of distinctive overshooting and regions of high vertical shear at various elevations above the ground; their presence indicated the complicated nature of the interaction of the stratified flow and the rugged terrain. Laminar flows were observed in most of the region, except in the thin layer adjacent to the ground where turbulent flows exist.

(ii) The plumes rapidly rise to their terminal heights and level off. The plumes are basically turbulent, but tend to relaminarize far downstream of the stack.

(iii) Under the conditions simulated, the plumes are aloft upstream of the mountains. No direct impingement is observed on the upstream sides of the mountains.

(iv) Downslope winds traced by the plumes are observed in the lees of the mountains for all four models. The pollutants in the plumes are carried closer to the leeward mountain slopes by the downslope wind.

(v) Generation of lee waves is demonstrated by several traces of the plumes (figs. 6b, 6c, 8b and 8c). For the same model, the wavelength decreases with a decreasing Froude number. Downstream of the first wave trough, the vertical spreads begin to increase (figs. 6b and 8b). The waves tend to break off for low internal-Froude-number cases, and abrupt enlargement of the plume size occurs farther downstream (figs. 5b, 7c, 8c, 5d and 8f).

(vi) Close to the surface of the leeward mountain slopes, the terrain effect on plume dispersion is strong. The plume is carried around the mountain peak (fig. 7f). In other cases, the plume is diverted from the wind direction and is forced to meander along a valley (figs. 8e and 8f) on the leeward side of the mountain.

(vii) Ground concentrations as high as 4 ppm are measured at, and downstream of, the locations where downslope winds occur, and the plumes are brought into direct contact with the ground (figs. 5b, 7b and 7c).

(viii) Based on the results of this laboratory simulation, we recommend that full-scale samplers be installed in areas where high ground concentrations are likely to occur.

References

Briggs, G. A. (1969) Plume Rises, U.S. Atomic Energy Commission Critical Review Series, TID-25072.

Counihan, J. (1969) "An Improved Method of Simulating an Atmospheric Boundary Layer in a Wind Tunnel," Atmospheric Environment 3, 197-214.

Davenport, A. G. (1961) "The Spectrum of Horizontal Gustiness Near the Ground in High Winds," Quart. J. Roy Meteorol. Soc. 87, 194.

Hinze, J. O. (1959) Turbulence, McGraw-Hill Book Company, Inc., New York.

Hoult, D. P. and Weil, J. W. (1972) "Turbulent Plume in a Laminar Cross Flow," Atmospheric Environment 6, 513-531.

Lin, J. T., Liu, H. T., Pao, Y. H., Lilly, D. K., Israeli, M. and Orszag, S. A. (1974) "Laboratory and Numerical Simulation of Plume Dispersion in Stably Stratified Flow Over Complex Terrain," Report No. 654/4-74-044, USEPA, Research Triangle Park, North Carolina.

Liu, H. T. and Karaki, S. (1973) "Studies of Particulate Plume Diffusion Over Laboratory Wind-Generated Water Waves," Atmospheric Environment 7, 869-890.

Liu, H. T., Lin, J. T., Pao, Y. H., Veenhuizen, S. D., Peecher, D. W. and Hiatt, G. L. (1974) The Plume Dispersion in Stably Stratified Flow Over a Flat Plate and a Three-Dimensional Terrain, Flow Research Film No. 6.

Liu, H. T., and Lin, J. T. (1975) "Laboratory Simulation of Plume Dispersion in Stably Stratified Flows Over Complex Terrain, Phase 2," Flow Research Report No. 57.

Liu, H. T., Lin, J. T., Peecher, D. W. and Shearer, W. C. (1975) "Laboratory Simulation of Plume Dispersion from a Lead Smelter: Glover, Missouri," Flow Research Film No. 8.

Orgill, M. M., Cermak, J. E. and Grant, L. O. (1971) "Laboratory Simulation and Field Estimates of Atmospheric Transport-Dispersion Over Mountainous Terrain," Technical Report CER70-71MMO-HEC-LOG40, Colorado State University.

Lumley, J. L. and Panofsky, H. A. (1964) The Structure of Atmospheric Turbulent, Datascience Publishers, New York.

Pao, Y. H., Lin, J. T., Carlson, R. L. and Smithmeyer, L. P. C. (1971) "The Design and Construction of a Stratified Towing Tank with an Oil-Lubricated Carriage," Flow Research Report No. 4 (APL/JHU POR-3530).

Plate, E. J. (1971) Aerodynamic Characteristic of Atmospheric Boundary Layers, AEC Critical Review Series.

Schiermeier, F. A. and Niemeyer, L. E. (1968) "Large Power Plant Efflucent Study" (LAPPES), Vol. 1 - Instrumentation, Procedures, and Data Tabulations, National Air Pollution Control Administration Publication No. APTD70-2.

Schlichting, H. (1968) Boundary Layer Theory, 6th Edition, Mc-Graw Hill Book Company, New York.

Sedov, L. I. (1959) Similarity and Dimensional Methods in Mechanics, Academic Press, New York and London.

Shea, E. P. (1973) "Emissions from Lead Smelter at American Smelting and Refining Company, Glover, Missouri," Report No. EMB 73-PLD-1, USEPA, Research Triangle Park, North Carolina.

Slade, D. H. (1969) "Low Turbulence Flow in the Planetary Boundary Layer and Its Relations to Certain Air Pollution Problems," J. of Applied Meteorology 8, 514-522.

Turner, J. S. (1973) Buoyancy Effects in Fluids, Cambridge University Press, Cambridge.

Veenhuizen, S. D., Lin, J. T., Pao, Y. H., Peecher, D. W. and Hiatt, G. L. (1973) "Laboratory Simulation of Plumes from Kennecott Copper Smelters in Garfield, Utah: Neutral Atmosphere," Flow Research Report No. 9.

Yu, H. Y. and Lin, J. T. (1975) "A Technique for Generating a Turbulent Boundary Layer in a Wind-Wave Tank, Flow Research Note No. 71, presented at 2nd U.S. National Conference on Wind Engineering Research, 23-25 June, 1975, Colorado State University, Fort Collins, Colorado (APL/JHU POR-3663).

TABLE 1 PHYSICAL DATA OF THE STACK AND THE EFFLUENT

DESCRIPTION	FIELD		LABORATORY	
Stack Height H [m]	186		7.4×10^{-2}*	
Stack Diameter D [m]	3.66		1.5×10^{-3}*	
Effluent Temperature θ_s [^oK]	375		363	
	Neutral	Stable	Neutral	Stable
Ambient Temperature θ_a [^oK]	303	273	293	293
Ambient Pressure p_a [$Kgfm^{-2}$]	9.59×10^3	9.56×10^3	1.06×10^4	1.06×10^4
Ambient Density ρ_a [$Kgfs^2m^{-4}$]	1.10×10^{-1}	1.22×10^{-1}	1.0×10^3	1.01×10^3
Effluent Density ρ_a [$Kgfs^2m^{-4}$]	8.9×10^{-2}	8.9×10^{-2}	1.17×10^3	1.17×10^3
Effluent Speed W_s [$m\varepsilon^{-1}$]	1.12×10^1	1.12×10^1	1.76×10^{-1}	1.33×10^{-1}

*Based on 1/2500 scale

TABLE 2 SIMULATION CONDITIONS

Run No.	Brunt-Vaisala Frequency N [Hz]		Lapse Rate Γ [°C/m]	Free-stream Wind Speed U_∞ [m/s]		Boundary Layer Thickness δ [m]		Wind Direction	Speed Ratio K	Internal Froude Number F_H	Stack Froude Number F_D
	Field	Laboratory	Field	Field	Laboratory	Field	Laboratory				
Ia	0	0	-.0098	8.0	.126	675	.27	112°	1.4	∞	3.9
Ib	.0061	.18	.031	2.5	.03	--	--	112°	4.4	2.2	3.1
IIa	0	0	-.0098	8.	.126	550.	.22	163°	1.4	∞	3.9
IIb	.0050	.15	.018	5.0	.06	--	--	163°	2.2	5.4	3.0
IIc	.0050	.15	.018	2.5	.03	--	--	163°	4.4	2.7	3.0
IIIa	0	0	-.0098	8.0	.126	588	.24	206°	1.4	∞	3.9
IIIb	.0050	.15	.018	5.0	.06	--	--	206°	2.2	5.4	3.1
IIIc	.0050	.15	.018	2.5	.03	--	--	206°	4.4	2.7	3.1
IVa	0	0	-.0098	8.0	.126	588	.24	245°	1.4	∞	3.9
IVb	.0050	.15	.018	5.0	.06	--	--	245°	2.2	5.4	3.1
IVc	.0050	.15	.018	2.5	.03	--	--	245°	4.4	2.7	3.1

TABLE 3 DATA OF GROUND CONCENTRATIONS

RUN Ib

Thermister Probe Number	x [km]	y [m]	z [m]	$\bar{\theta}$ [°C]	$\frac{\bar{\theta}-\bar{\theta}_a}{\bar{\theta}_s-\bar{\theta}_a}$	$\sqrt{\overline{\theta^2}}$ [°C]
1	2.1	0	360	20.47*	0	1.1×10^{-3}**
2	4.3	91	375	20.48	1.4×10^{-4}	2.6×10^{-3}
3	5.3	101	457	20.50	4.3×10^{-4}	2.4×10^{-3}
4	5.5	61	485	20.53	8.6×10^{-4}	3.9×10^{-3}
5	5.3	162	486	20.53	8.6×10^{-4}	2.9×10^{-3}
6	5.5	0	483	20.51	5.8×10^{-4}	4.9×10^{-3}
7	5.9	61	448	20.52	7.2×10^{-4}	2.4×10^{-3}
8	6.1	61	375	20.53	8.6×10^{-4}	3.6×10^{-3}
9	6.7	91	314	20.50	4.3×10^{-4}	5.9×10^{-3}
10	6.8	91	351	20.50	4.3×10^{-4}	8.3×10^{-3}

RUN IIIb

Thermister Probe Number	x [km]	y [m]	z [m]	$\bar{\theta}$ [°C]	$\frac{\bar{\theta}-\bar{\theta}_a}{\bar{\theta}_s-\bar{\theta}_a}$	$\sqrt{\overline{\theta^2}}$ [°C]
7	4.4	61	469	-	----	----
6	4.5	76	488	19.61	1.4×10^{-4}	1.4×10^{-3}
5	4.7	91	512	19.60*	0	9.7×10^{-4}**
4	4.9	91	512	19.60	0	1.1×10^{-3}
3	5.3	76	494	19.61	1.4×10^{-4}	4.9×10^{-4}
2	5.5	76	457	19.66	8.5×10^{-4}	1.4×10^{-3}
8	5.6	122	415	19.66	8.5×10^{-4}	5.7×10^{-4}
1	5.8	76	418	19.67	9.9×10^{-4}	1.1×10^{-3}
9	6.2	0	329	19.74	2.0×10^{-3}	2.1×10^{-3}
10	6.5	0	338	19.74	2.0×10^{-3}	2.0×10^{-3}

RUN IIIc

Thermister Probe Number	x [km]	y [m]	z [m]	$\bar{\theta}$ [°C]	$\frac{\bar{\theta}-\bar{\theta}_a}{\bar{\theta}_s-\bar{\theta}_a}$	$\sqrt{\overline{\theta^2}}$ [°C]
7	4.4	61	469	-	---	----
6	4.5	76	488	19.58*	0	2.2×10^{-3}
5	4.7	91	512	-	---	----
4	4.9	91	512	-	---	----
3	5.3	76	494	19.61	4.3×10^{-4}	5.2×10^{-3}
2	5.5	76	457	19.67	1.3×10^{-3}	2.9×10^{-3}
8	5.6	122	415	19.67	1.3×10^{-3}	2.1×10^{-3}
1	5.8	76	418	19.66	1.1×10^{-3}	2.4×10^{-3}
9	6.2	0	329	19.67	1.3×10^{-3}	2.4×10^{-3}
10	6.5	0	338	19.67	1.3×10^{-3}	3.9×10^{-3}

* Average Ambient Temperature

** Ambient Noise Level

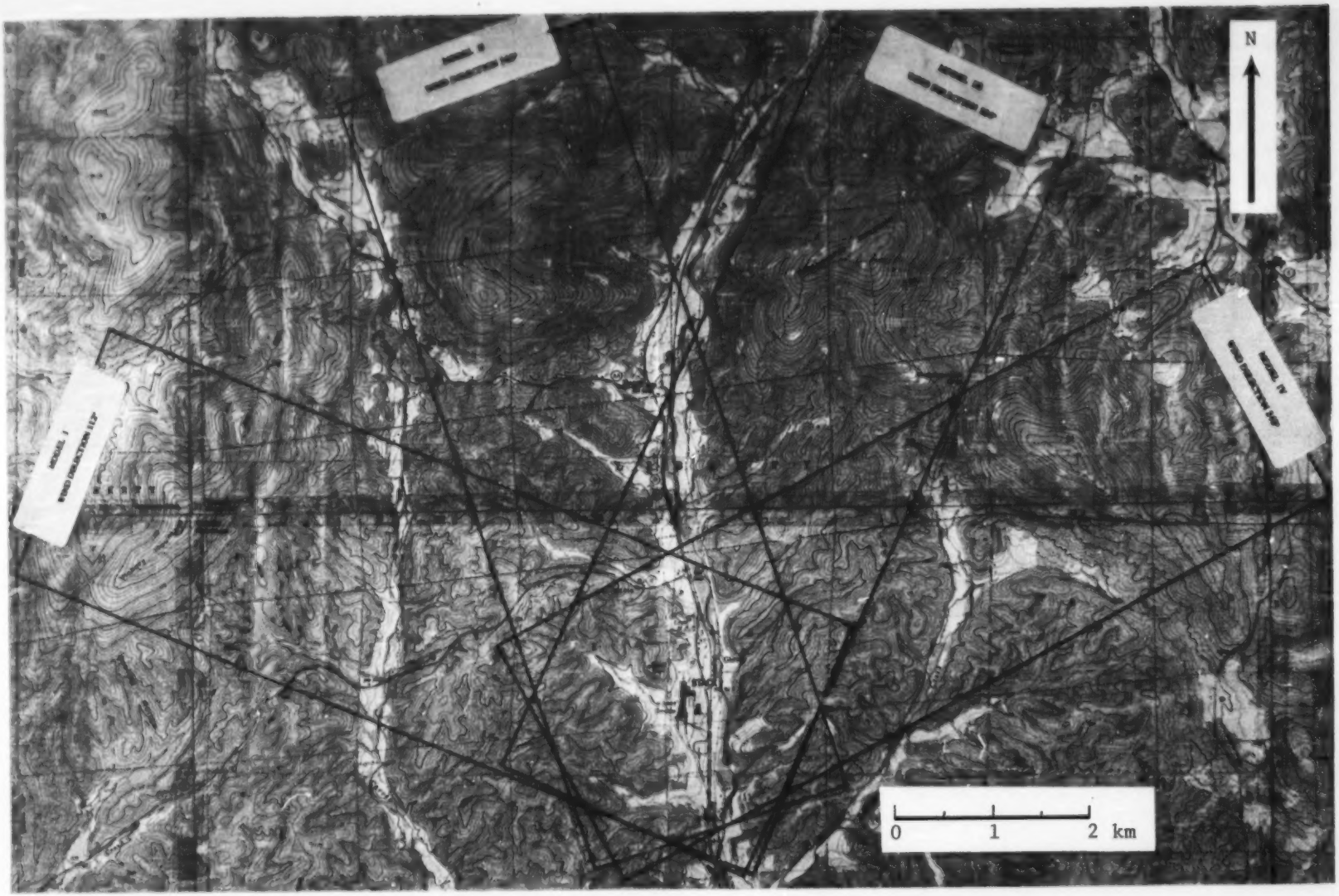

Fig. 1 A Contour Map of the Vicinity of the ASARCO Plant at Glover, Missouri

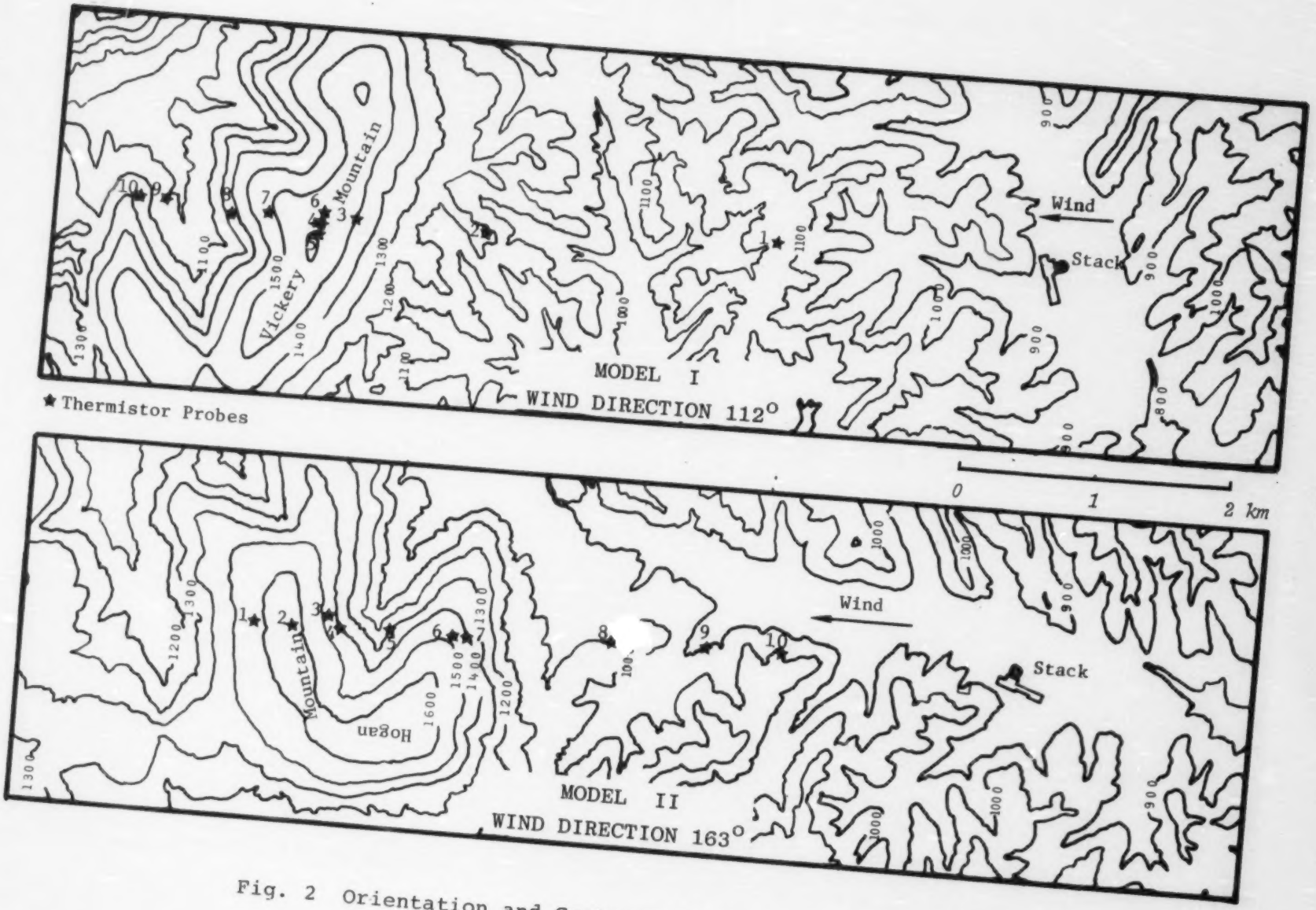

Fig. 2 Orientation and Contours of the Four Terrain Models

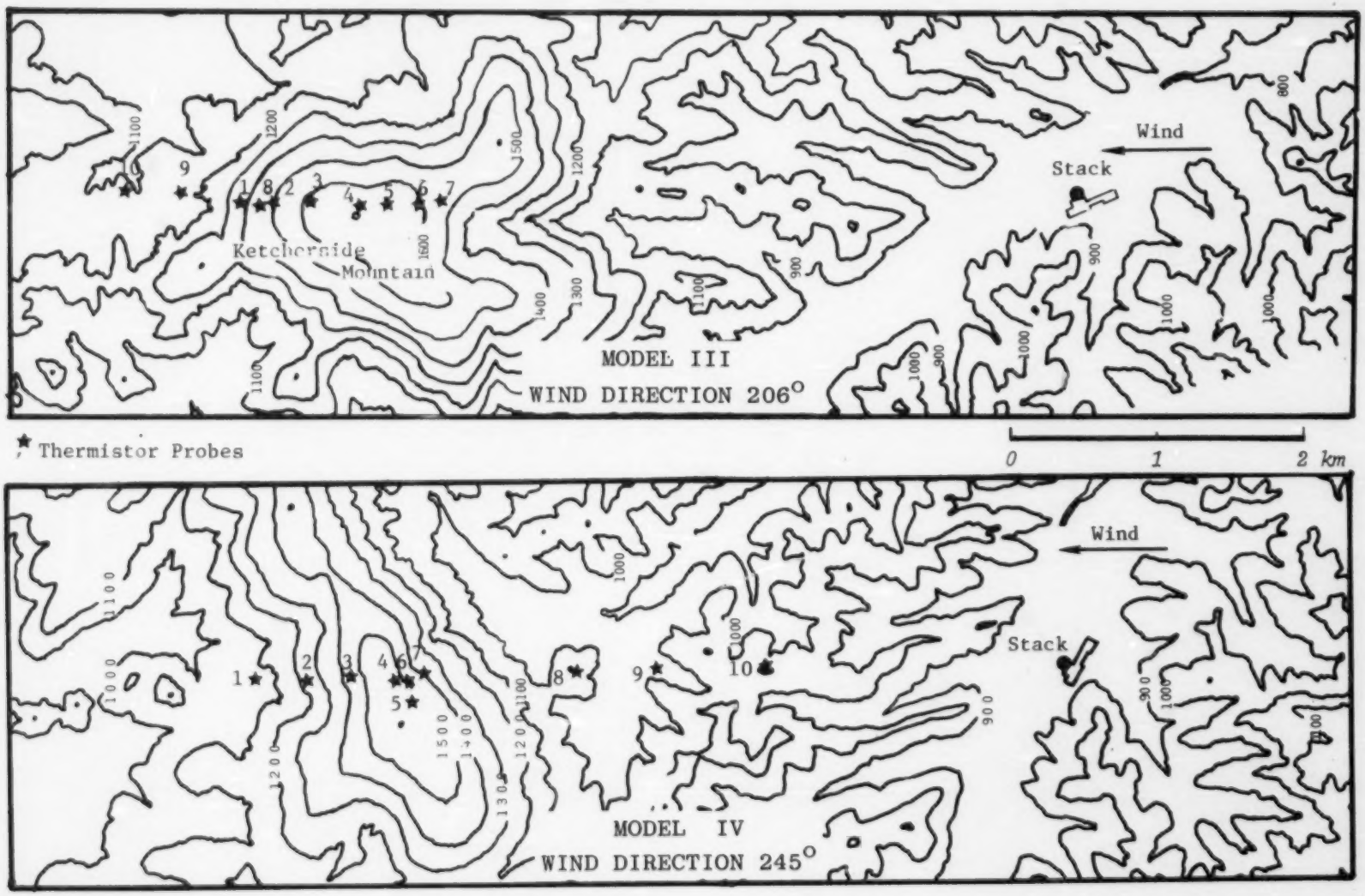

Fig. 2 (cont'd) Orientation and Contours of the Four Terrain Models

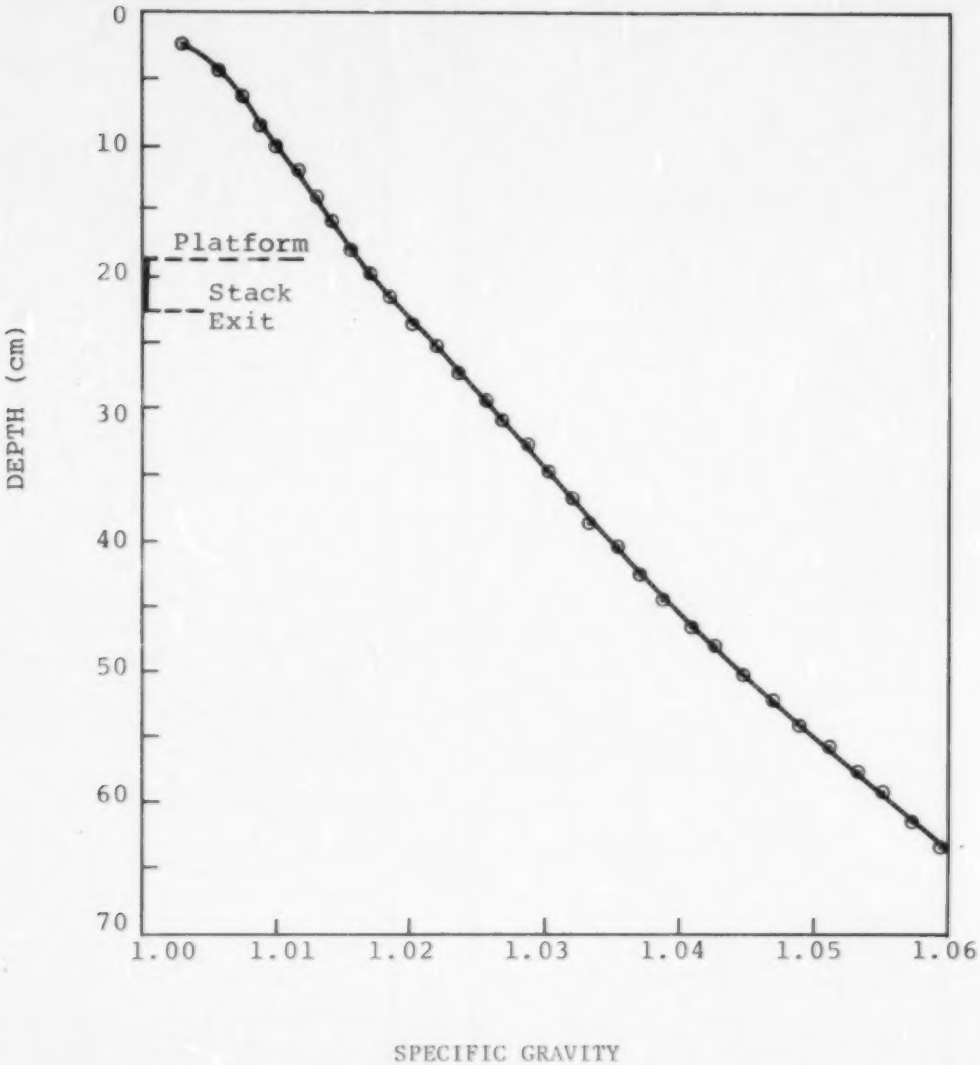

Fig. 3 A Stratification Profile Measured with a Conductivity Probe in the Towing Tank (Run IVb)

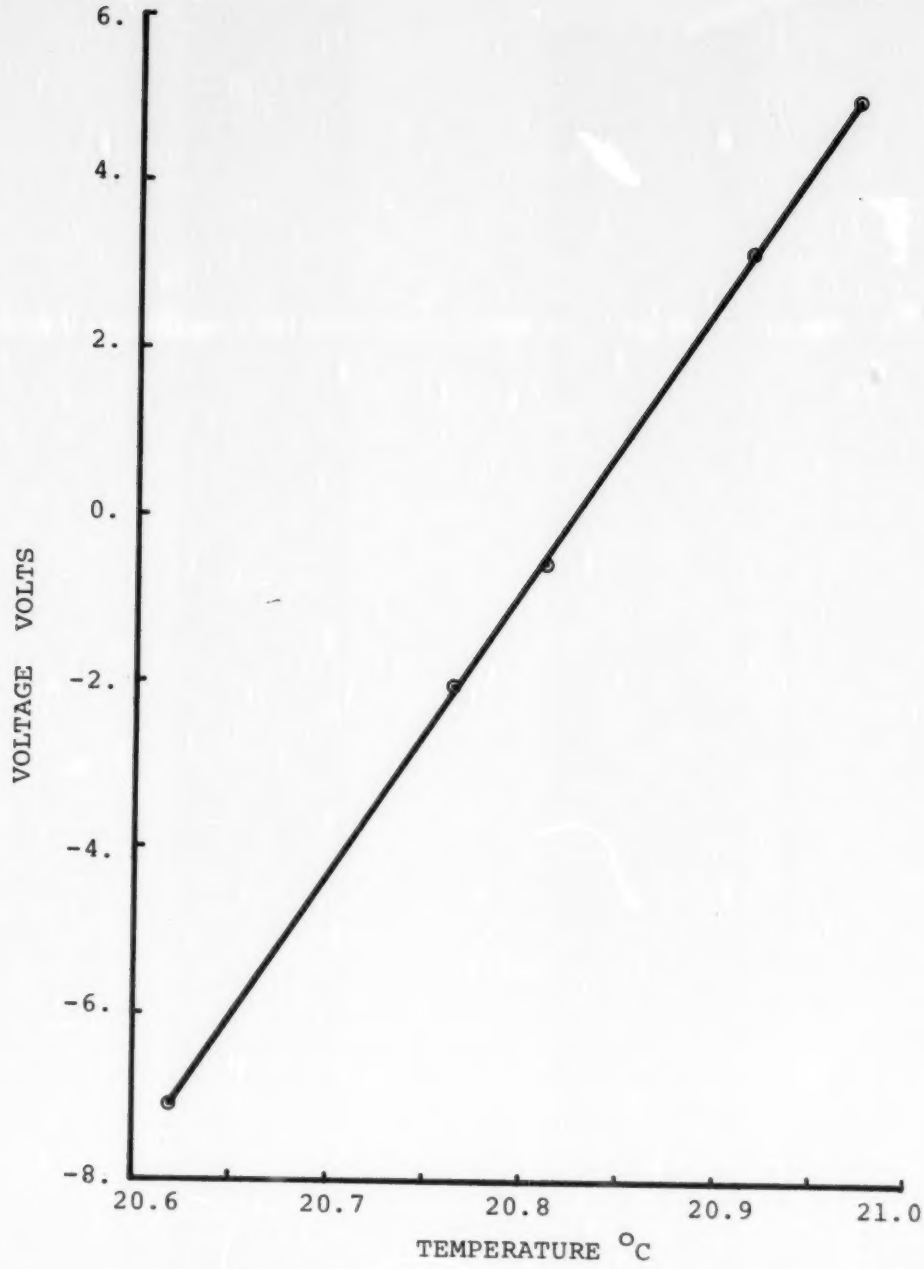

Fig. 4 A Calibration Curve of a Thermistor Probe (Run IVb)

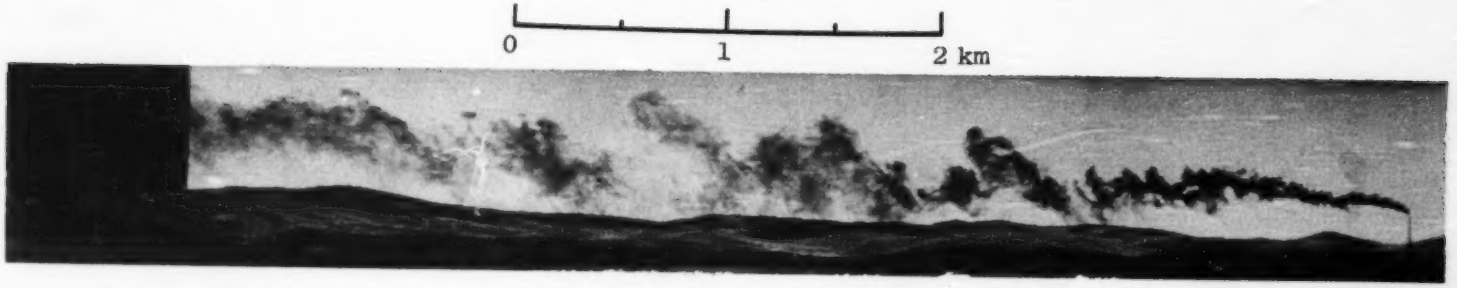

a. Run Ia: Neutral Condition, N = 0 Hz, U_∞ = 12.6 cm/s, K = 1.4, $F_H = \infty$, and F_D = 3.9

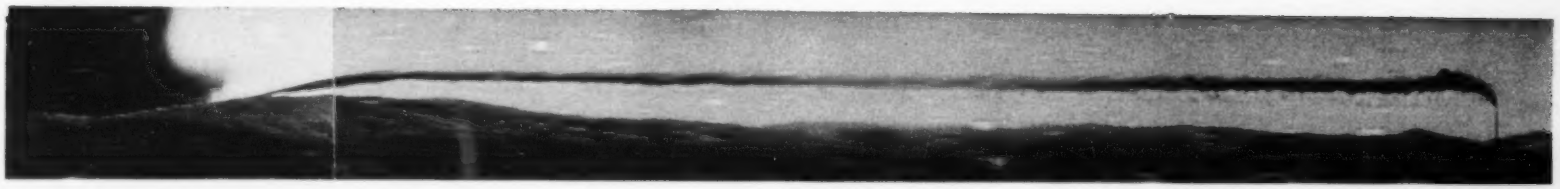

b. Run Ib: Stable Condition, N = .18 Hz, U_∞ = 3 cm/s, K = 4.4, F_H = 2.2, and F_D = 3.1

Fig. 5 Visualization Results of Run I: Side View

Wind Direction = 112°

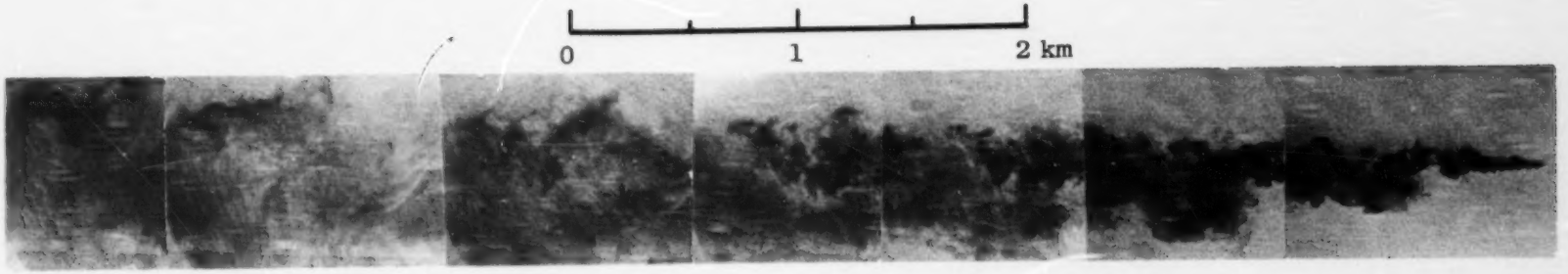

c. Run Ia: Neutral Condition, N = 0 Hz, U_∞ = 12.6 cm/s, K = 1.4, $F_H = \infty$, and F_D = 3.9

d. Run Ib: Stable Condition, N = .18 Hz, U_∞ = 3 cm/s, K = 4.4, F_H = 2.2, and F_D = 3.1

Fig. 5 (cont'd). Visualization Results of Run I: Plan View

Wind Direction = 112°

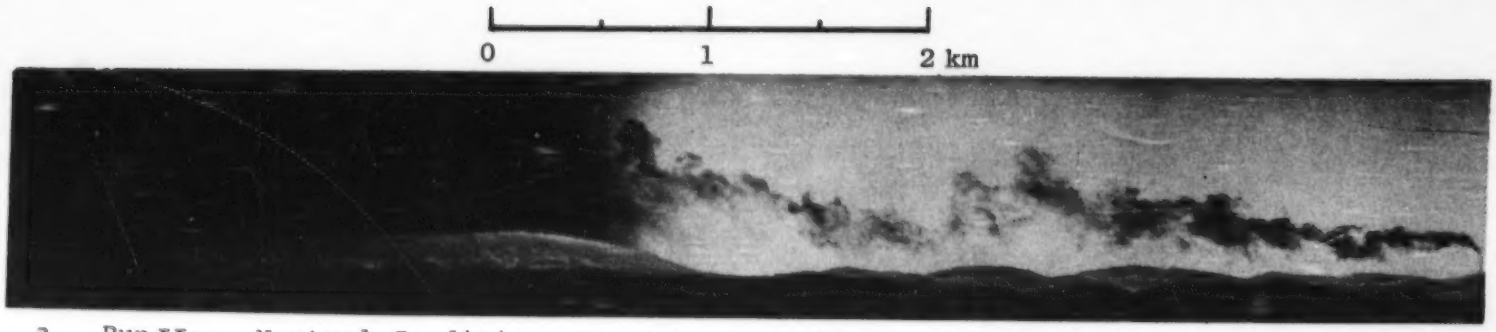

a. Run IIa: Neutral Condition, N = 0 Hz, U_∞ = 12.6 cm/s, K = 1.4, $F_H = \infty$, and F_D = 3.9

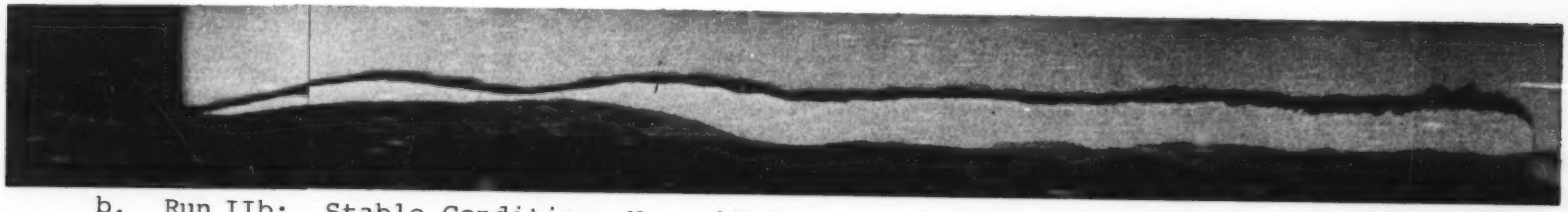

b. Run IIb: Stable Condition, N = .15 Hz, U_∞ = 6 cm/s, K = 2.2, F_H = 5.4, and F_D = 3.0

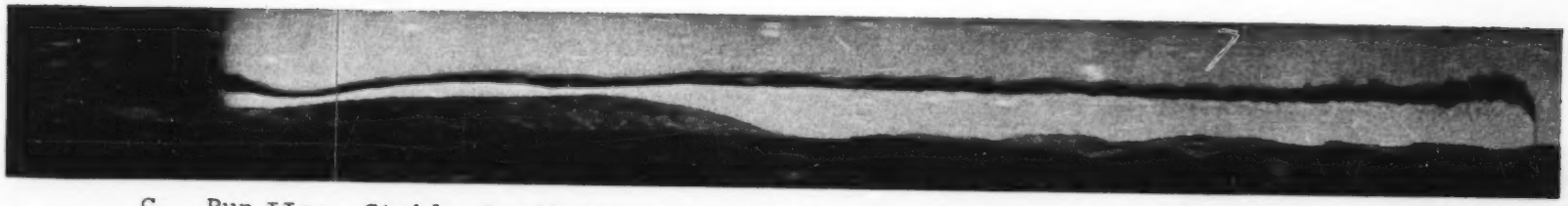

c. Run IIc: Stable Condition, N = .15 Hz, U_∞ = 3 cm/s, K = 4.4, F_H = 2.7, and F_D = 3.0

Fig. 6 Visualization Results of Run No. II: Side View
Wind Direction = 163°

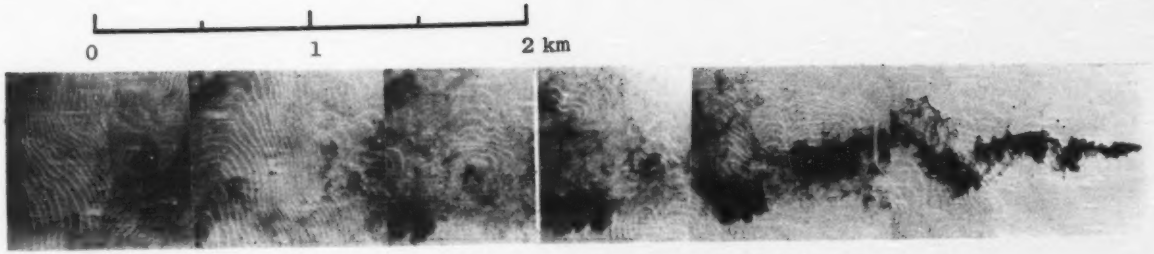

d. Run IIa: Neutral Condition, N = 0 Hz, U_∞ = 12.6 cm/s, K = 1.4, $F_H = \infty$, and F_D = 3.9

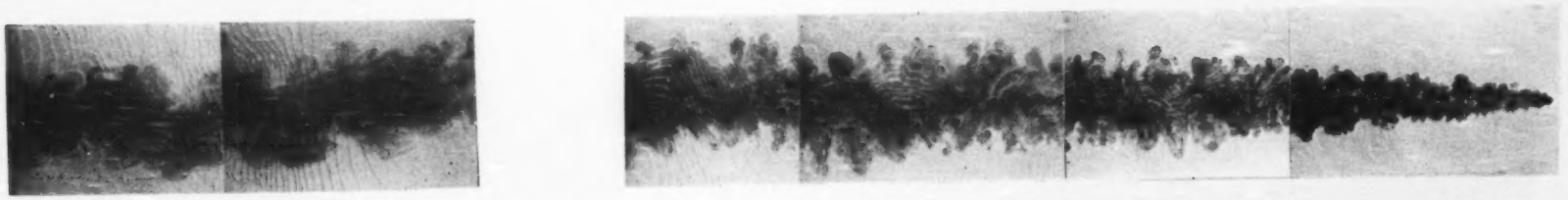

e. Run IIb: Stable Condition, N = .15 Hz, U_∞ = 6 cm/s, K = 2.2, F_H = 5.4, and F_D = 3.0

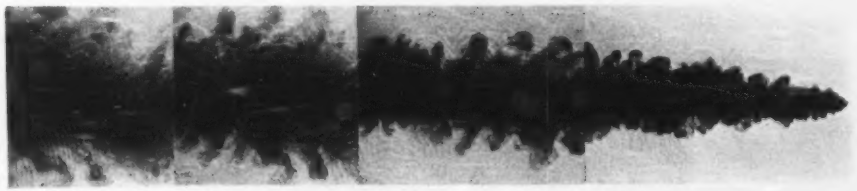

f. Run IIc: Stable Condition, N = .15 Hz, U_∞ = 3 cm/s, K = 4.4, F_H = 2.7, and F_D = 3.0

Fig. 6 (cont'd). Visualization Results of Run II: Plan View

Wind Direction = 163°

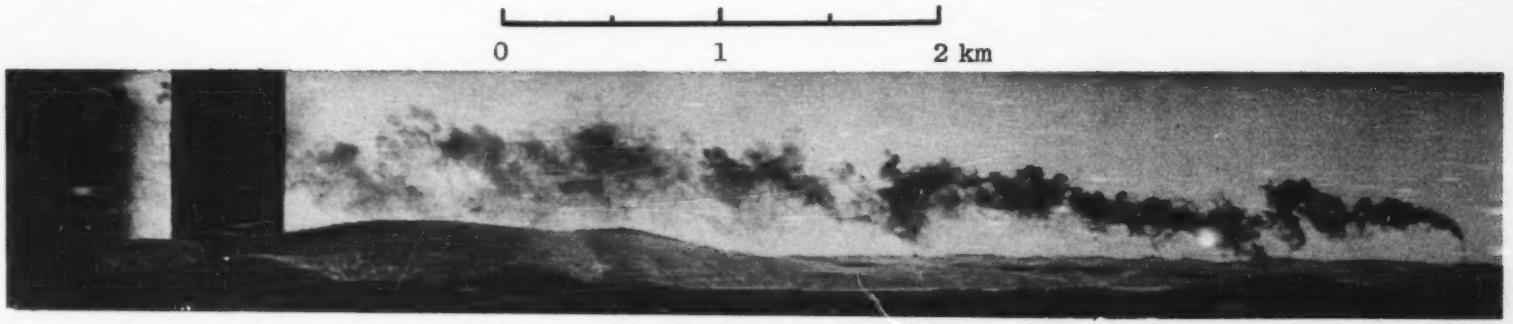

a. Run IIIa: Neutral Condition, N = 0 Hz, U_∞ = 12.6 cm/s, K = 1.4, $F_H = \infty$, and F_D = 3.9

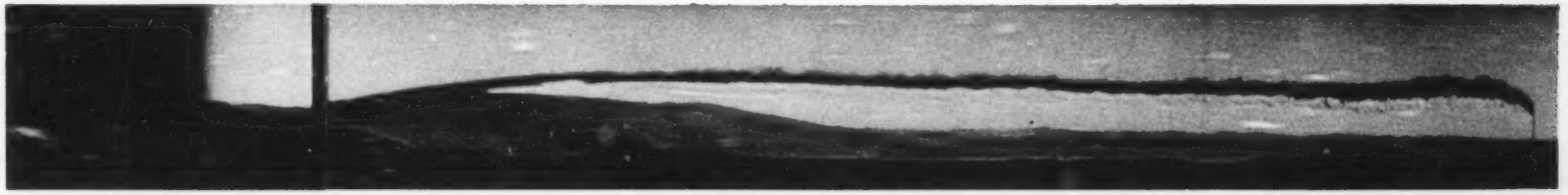

b. Run IIIb: Stable Condition, N = .15 Hz, U_∞ = 6 cm/s, K = 2.2, F_H = 5.7, and F_D = 3.1

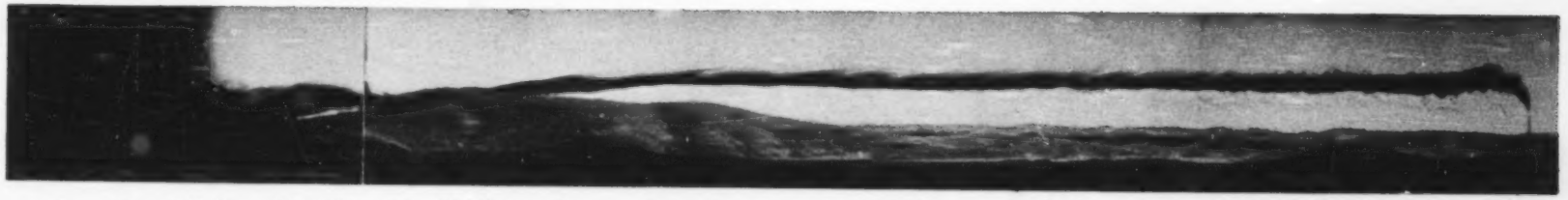

c. Run IIIc: Stable Condition, N = .15 Hz, U_∞ = 3 cm/s, K = 4.4, F_H = 2.7, and F_D = 3.1

Fig. 7 Visualization Results of Run III: Side View
Wind Direction =206°

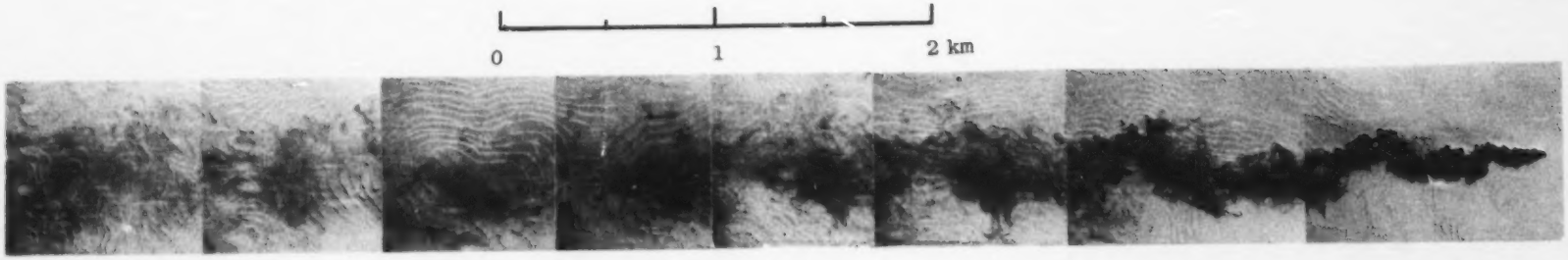

d. Run IIIa: Neutral Condition, N = 0 Hz, U_∞ = 12.6 cm/s, K = 1.4, F_H = ∞, and F_D = 3.9

e. Run IIIb: Stable Condition, N = .15 Hz, U_∞ = 6 cm/s, K = 2.2, F_H = 5.7, and F_D = 3.1

f. Run IIIc: Stable Condition, N = .15 Hz, U_∞ = 3 cm/s, K = 4.4, F_H = 2.7, and F_D = 3.1

Fig. 7 (cont'd). Visualization Results of Run III: Plan View

Wind Direction = 206°

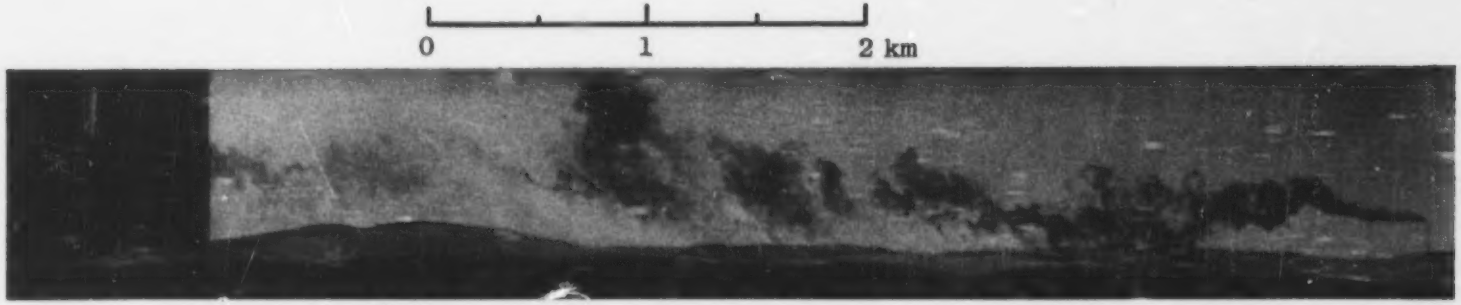

a. Run IVa: Neutral Condition, N = 0 Hz, U_∞ = 12.6 cm/s, K = 1.4, $F_H = \infty$, and F_D = 3.9

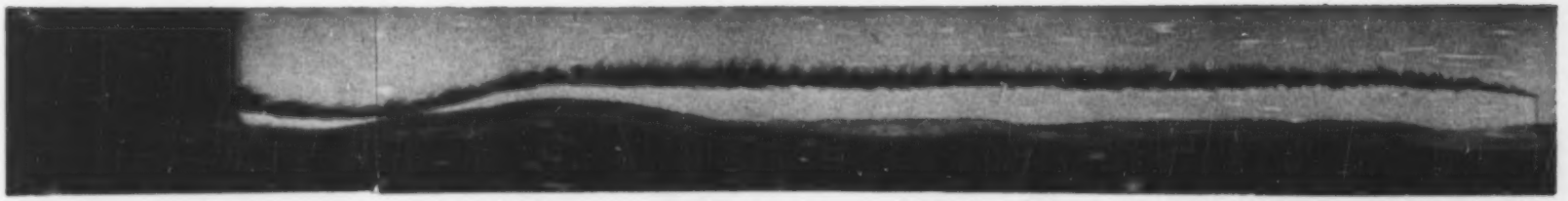

b. Run IVb: Stable Condition, N = .15 Hz, U_∞ = 6 cm/s, K = 2.2, F_H = 5.4, and F_D = 3.1

c. Run IVc: Stable Condition, N = .15 Hz, U_∞ = 3 cm/s, K = 4.4, F_H = 2.7, and F_D = 3.1

Fig. 8 Visualization Results of Run IV: Side View
Wind Direction = 245°

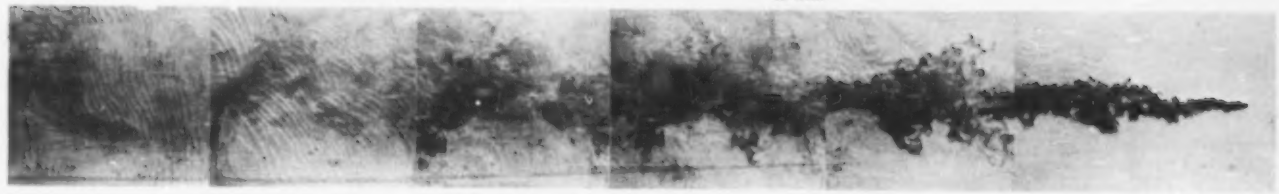

d. Run IVa: Neutral Condition, N = 0 Hz, U_∞ = 12.6 cm/s, K = 1.4, $F_H = \infty$, and F_D = 3.9

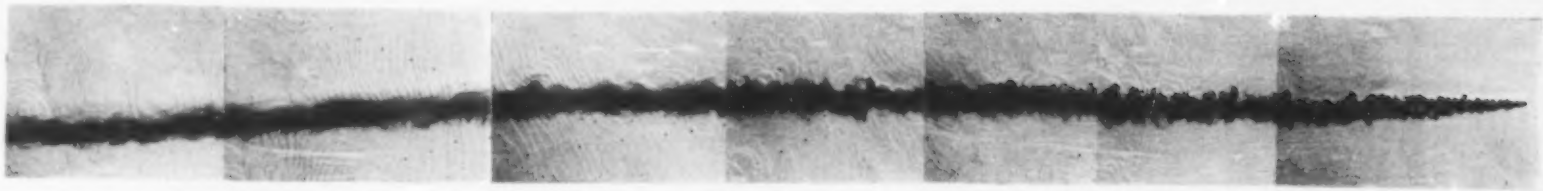

e. Run IVb: Stable Condition, N = .15 Hz, U_∞ = 6 cm/s, K = 2.2, F_H = 5.4, and F_D = 3.1

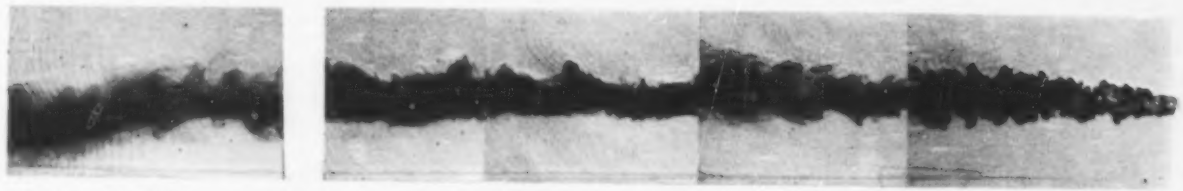

f. Run IVc: Stable Condition, N = .15 Hz, U_∞ = 3 cm/s, K = 4.4, F_H = 2.7, and F_D = 3.1

Fig. 8 (cont'd). Visualization Results of Run IV: Plan View

Wind Direction = 245°

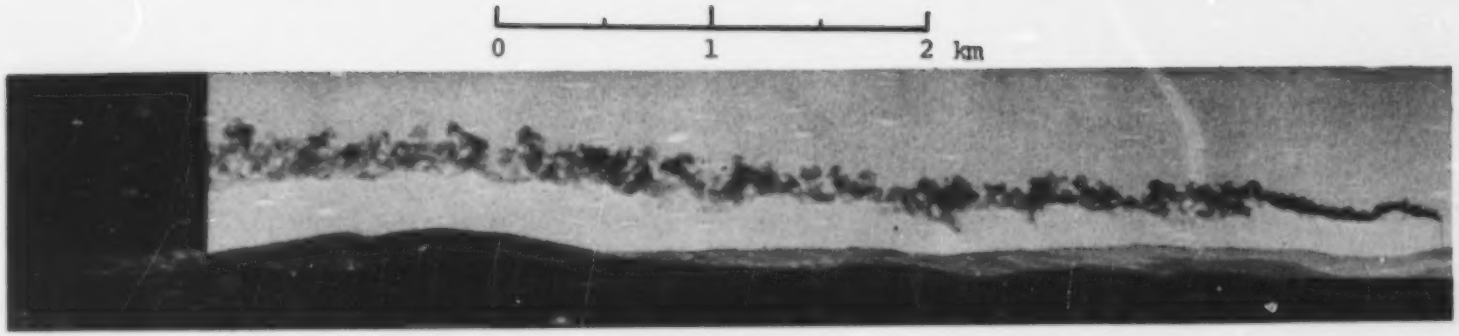

Fig. 9 Plume Dispersion Over Model IV (Wind Direction = 245°). The Picture Was Photographed Before the Turbulent Boundary Layer Was Fully Developed. See Fig. 7 for Comparison.

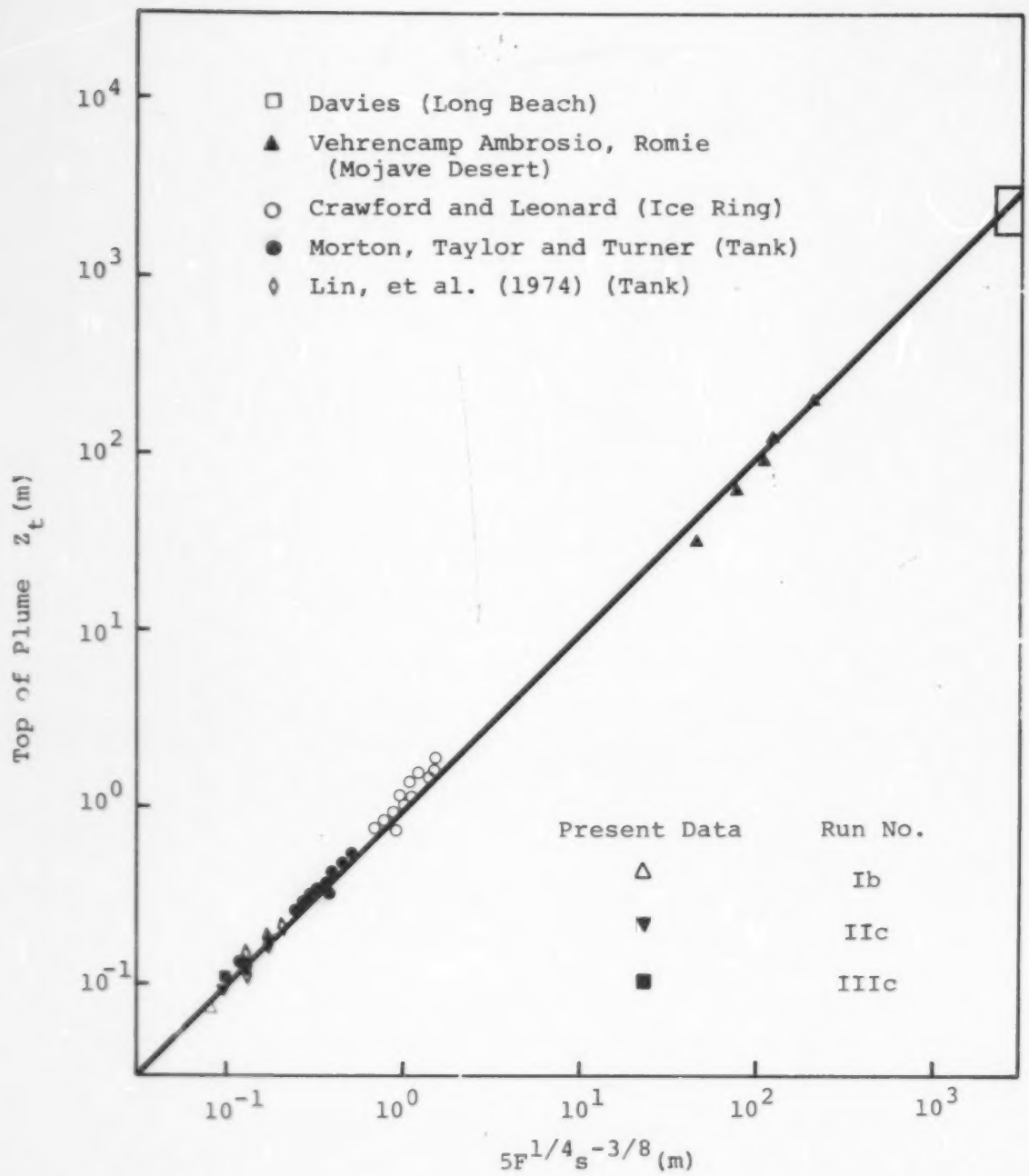

Fig. 10 Laboratory and Field Data of Plume Tops in Calm and Stable Flows (See Briggs, 1969)

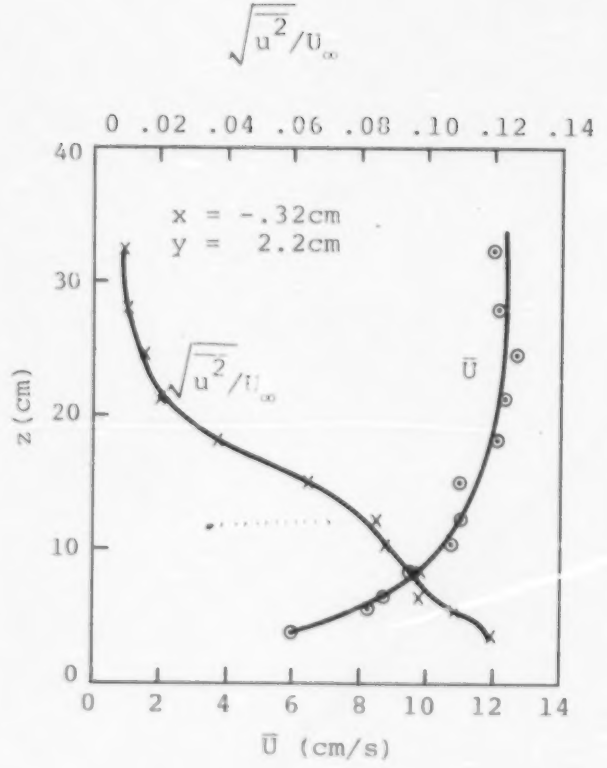

a. Run Ia, Wind Direction 112°

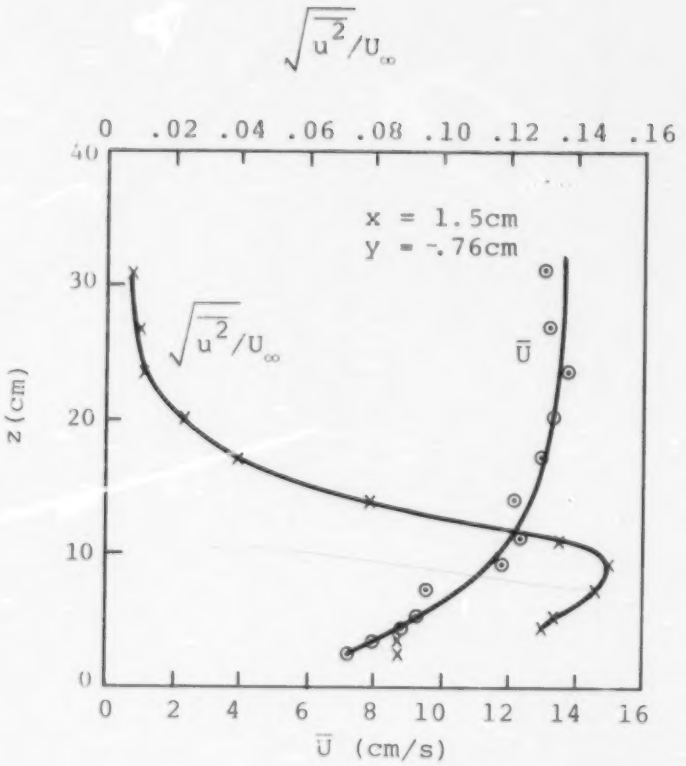

b. Run IIa, Wind Direction 163°

Fig. 11 Mean and Turbulent Velocity Profiles in the Vicinity of the Stack Under Neutral, High-Wind Conditions (U_∞ = 12.6 cm/s)

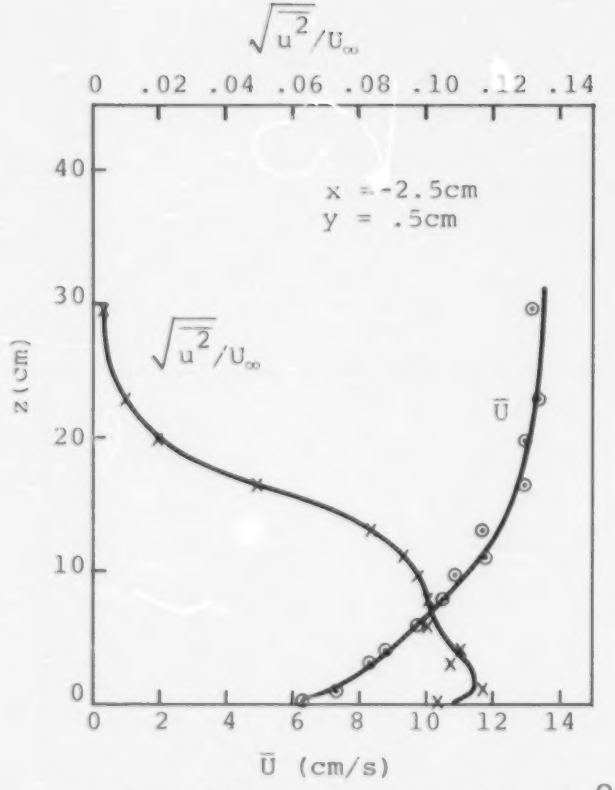

c. Run IIIa, Wind Direction 206°

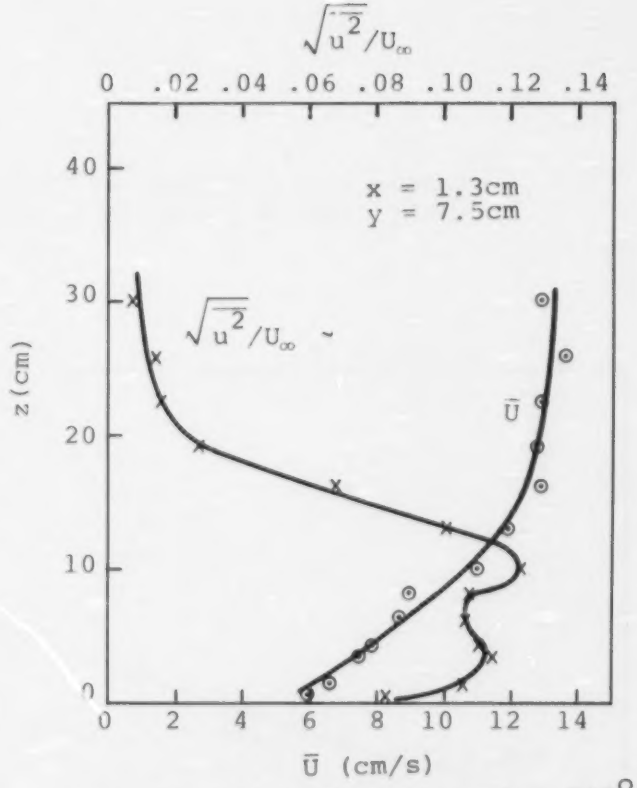

d. Run IVa, Wind Direction 245°

Fig. 11 (cont'd) Mean and Turbulent Velocity Profiles in the Vicinity of the Stack Under Neutral, High-Wind Conditions (U_∞ = 12.6 cm/s)

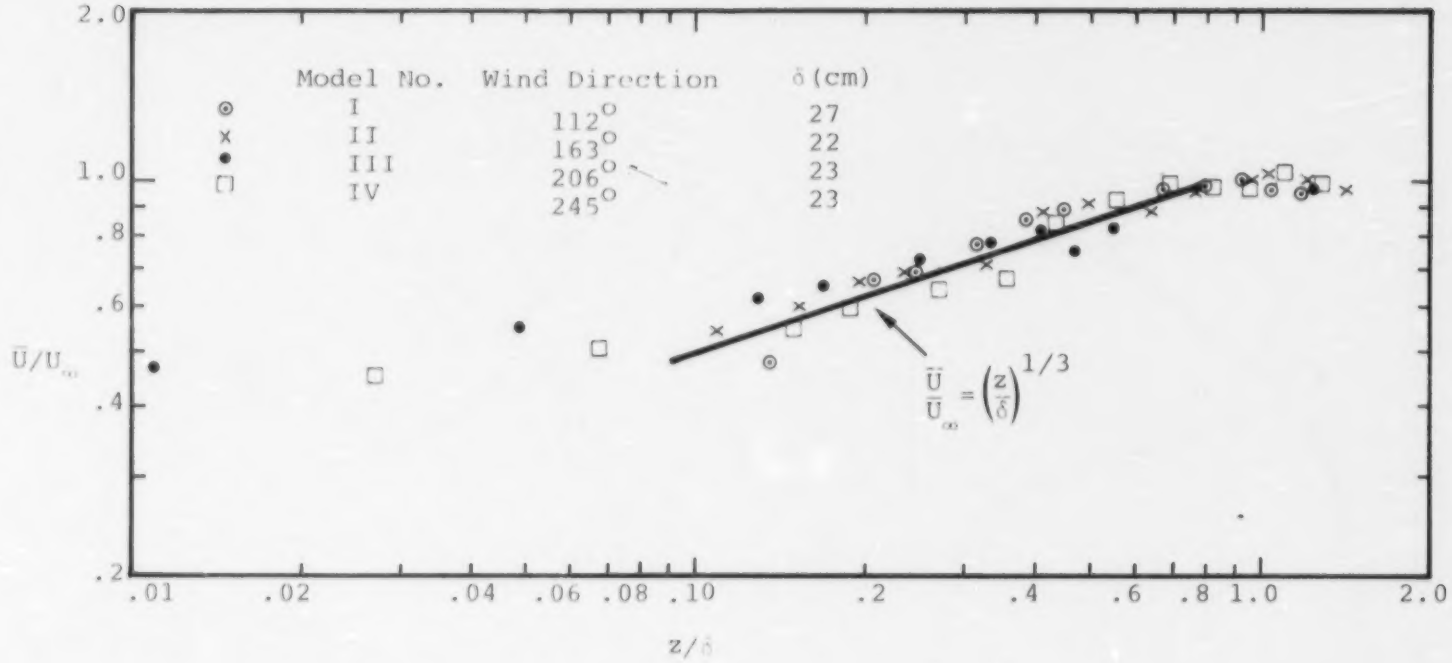

Fig. 12 Dimensionless Velocity Profiles Measured at the Vicinity of the Stack Over the Four Terrain Models Under Neutral Conditions

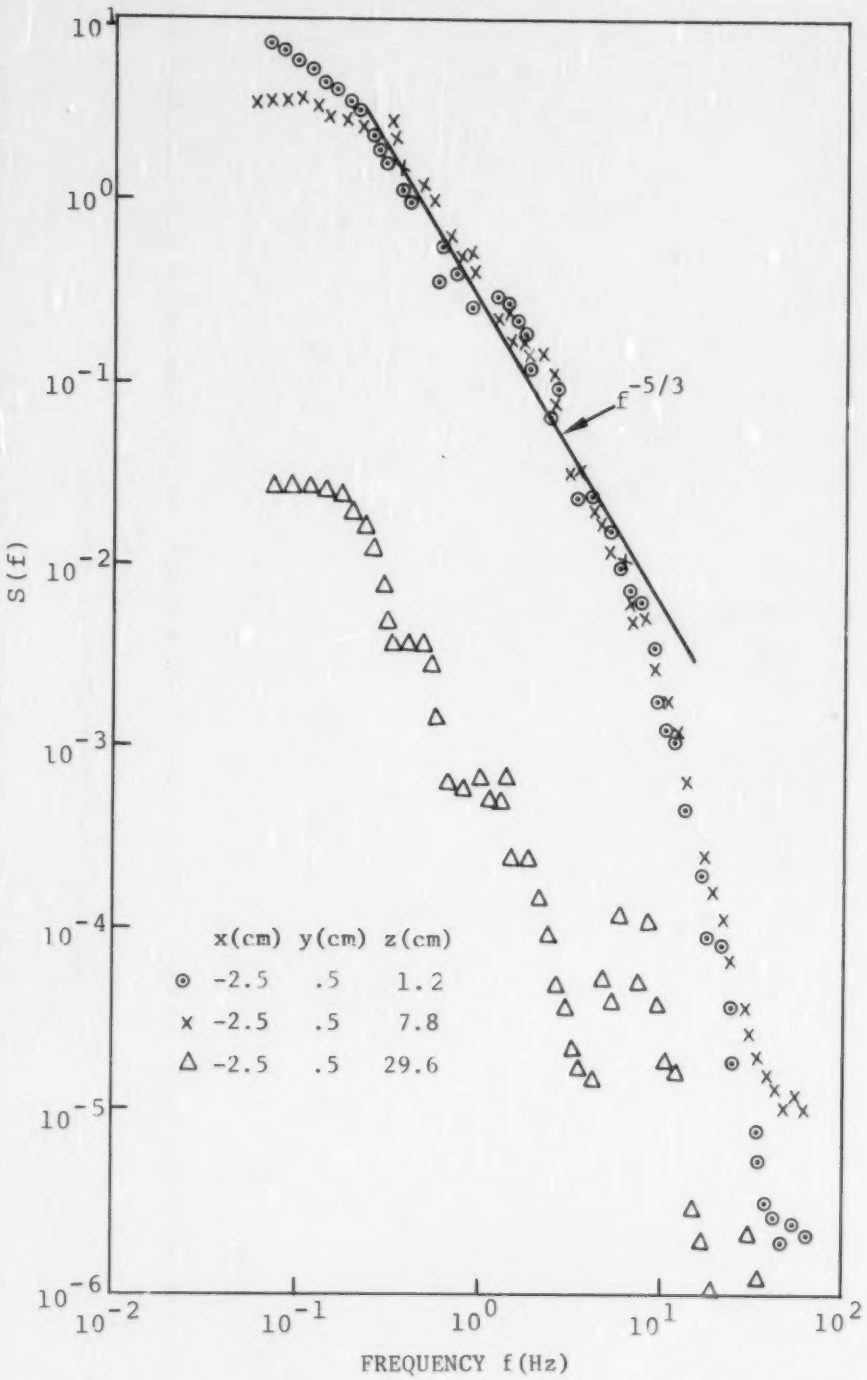

Fig. 13 One-Dimensional Spectra of Velocity Data Measured in the Vicinity of the Stack in Model III.

Wind Direction = 206° U_∞ = 12.6 cm/s

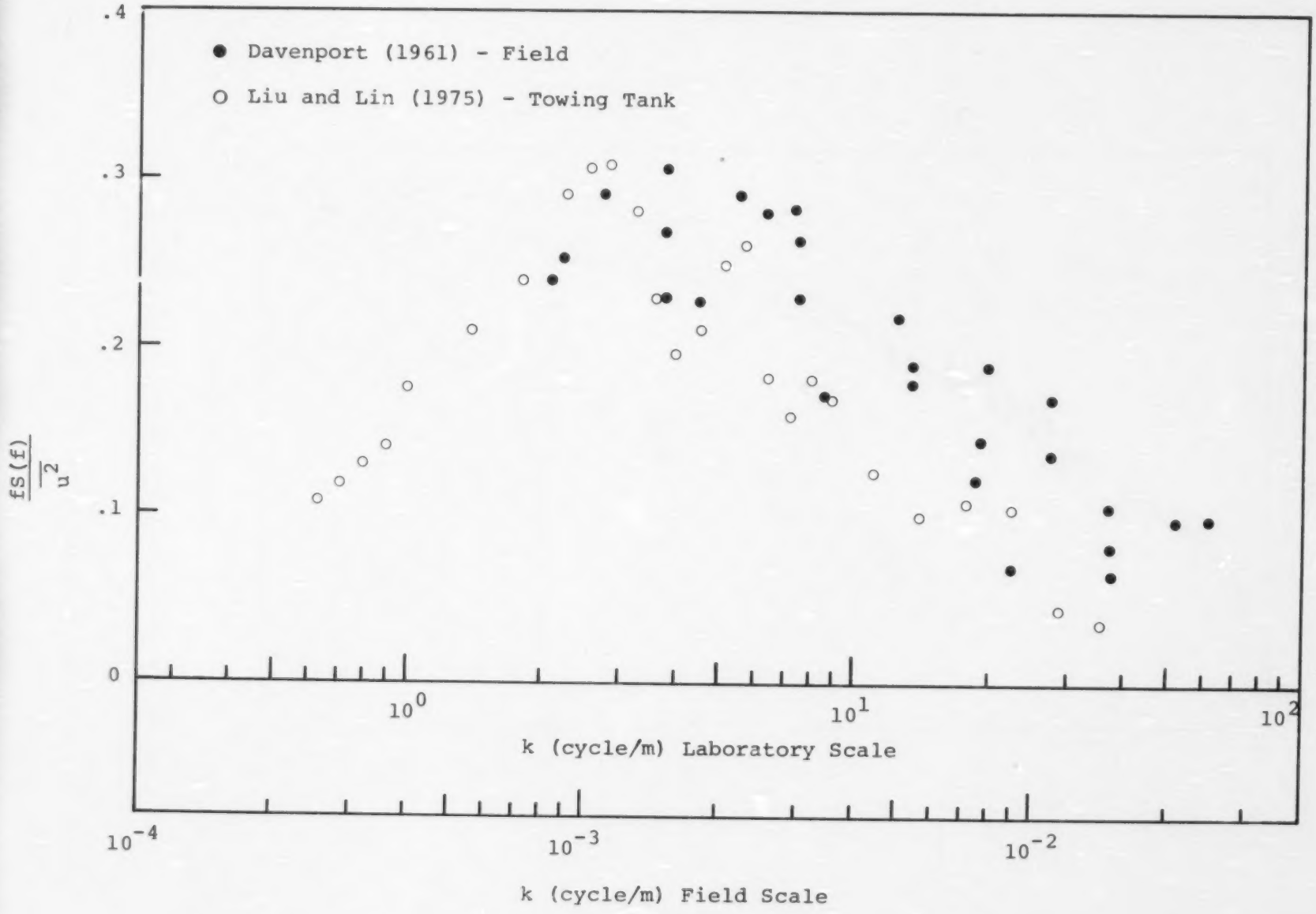

Fig. 14 Comparison Between Field and Laboratory Measurements of Turbulent Spectrum

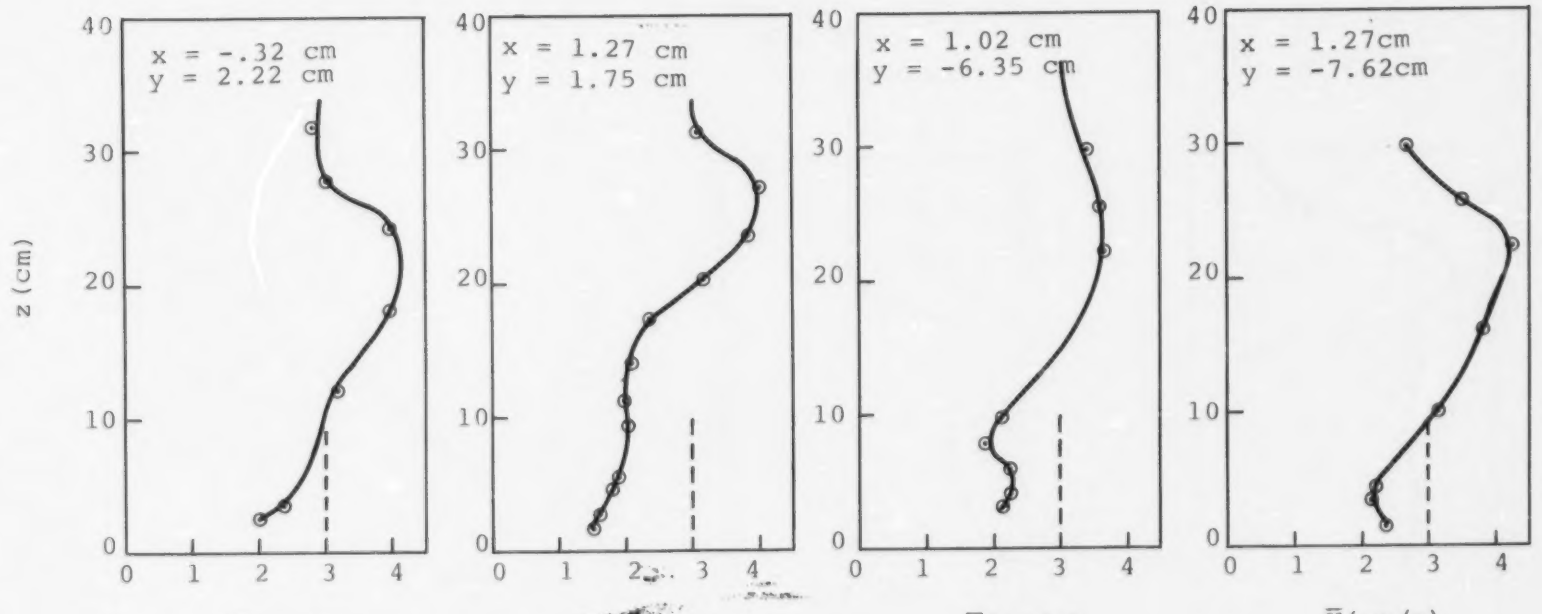

a. Run Ib, Wind Direction 112° F_H = 2.2

b. Run IIb, Wind Direction 163° F_H = 2.7

c. Run IIIb, Wind Direction 206° F_H = 2.7

d. Pun IVb, Wind Direction 245° F_H = 2.7

Fig. 15 Mean Velocity Profiles Under Stable Conditions
Low Internal-Froude-Number Cases

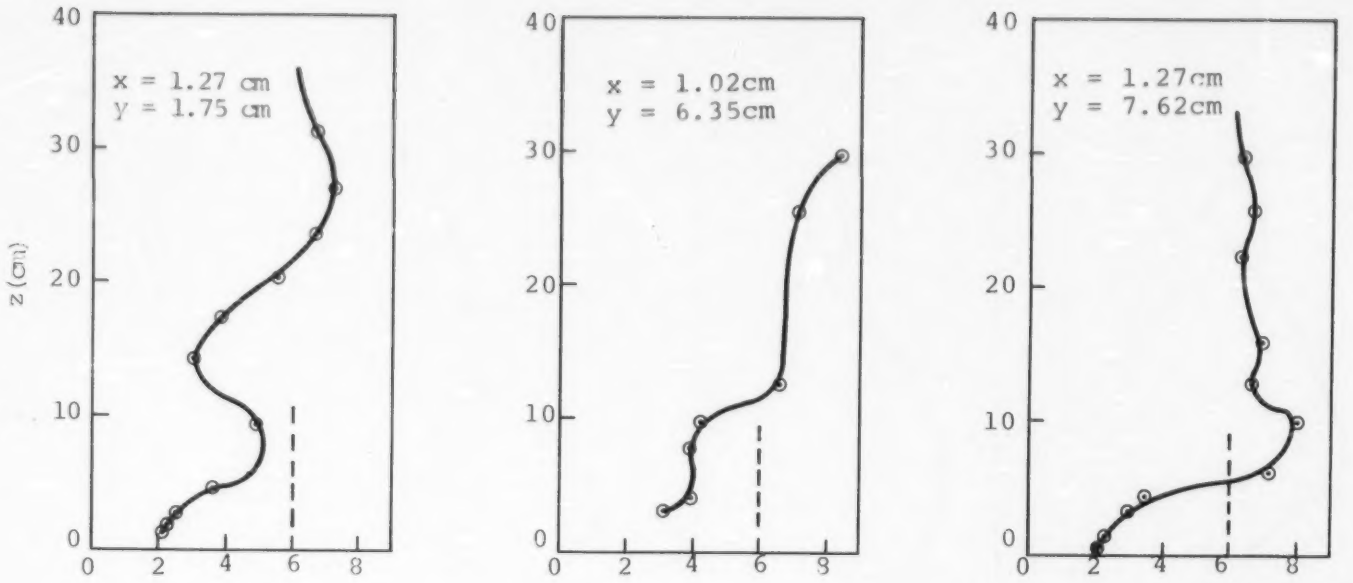

a. Run IIc, Wind Direction 163°

b. Run IIIc, Wind Direction 206°

c. Run IVc, Wind Direction 245°

Fig. 16 Mean Velocity Profiles Under Stable Conditions
High Internal-Froude-Number Cases, F_H = 5.4